THE EUROPEAN
PHYSICAL JOURNAL C

CrossMark

Static elliptic minimal surfaces in AdS₄

Georgios Pastras[a]

Institute of Nuclear and Particle Physics, NCSR "Demokritos", 15310 Aghia Paraskevi, Attiki, Greece

Abstract The Ryu–Takayanagi conjecture connects the entanglement entropy in the boundary CFT to the area of open co-dimension two minimal surfaces in the bulk. Especially in AdS₄, the latter are two-dimensional surfaces, and, thus, solutions of a Euclidean non-linear sigma model on a symmetric target space that can be reduced to an integrable system via Pohlmeyer reduction. In this work, we construct static minimal surfaces in AdS₄ that correspond to elliptic solutions of the reduced system, namely the cosh-Gordon equation, via the inversion of Pohlmeyer reduction. The constructed minimal surfaces comprise a two-parameter family of surfaces that include helicoids and catenoids in H³ as special limits. Minimal surfaces that correspond to identical boundary conditions are discovered within the constructed family of surfaces and the relevant geometric phase transitions are studied.

1 Introduction

The AdS/CFT correspondence [1–3] is a framework that connects theories which include gravitational dynamics in spacetimes with AdS asymptotics to conformal field theories defined on the AdS boundary. The similarity of the laws of black hole physics to those of thermodynamics suggests that the emergence of gravity in the bulk theory incorporates thermodynamics of some underlying degrees of freedom [4], which in the context of the AdS/CFT correspondence can be naturally selected to be the degrees of freedom of the boundary theory. Then gravity can be understood as an emergent entropic force originating from the strongly coupled CFT degrees of freedom.

The more recent point of view of gravity as an emergent entropic force suggests that gravity is not related with ther-

mal statistics but rather with quantum entanglement statistics. The original proposal was made by Ryu and Takayanagi [5,6] and its basic element is the RT conjecture. This states that the entanglement entropy of a subsystem of the degrees of freedom of the boundary CFT is mapped through the holographic correspondence to the area of an open minimal co-dimension two surface (A^{extr}) in the bulk geometry, anchored to the entangling surface in the boundary, i.e. the surface separating the subsystem from its environment,

$$S_{EE} = \frac{1}{4G_N} \text{Area}(A^{\text{extr}}). \tag{1.1}$$

This program has advanced a lot ever since [7–12], including an understanding of Einstein equations at linear order as directly emerging from the first law of entanglement thermodynamics [13–15]. A major difficulty in these calculations is the specification of the minimal surface for an arbitrary entangling surface, which arises from the non-linearity of the relevant equations. More specifically, closed forms for the minimal surface in more than three spacetime dimensions are known only for the case that the bulk geometry is pure AdS and furthermore the entangling surface encloses a region with the shape of a disk or an infinite strip.

Both the disk and the strip minimal surfaces are anchored to entangling surfaces characterized by trivial curvature. Furthermore, disk minimal surfaces are special in the sense that they have vanishing Gaussian curvature. The discovery of more general minimal surfaces, apart being interesting from a purely mathematical point of view, can provide a useful tool for the study of holographic entanglement entropy and its dependence on the geometry of the entangling surface. It can also provide a non-trivial check of the connection between Einstein equations and entanglement thermodynamics through the RT conjecture.

In the special case of AdS₄, the co-dimension two minimal surfaces that are related to the entanglement entropy via the RT conjecture are two-dimensional surfaces. Therefore, their area can be considered as the Euclidean analog

[a] e-mail: pastras@inp.demokritos.gr

of the Nambu–Goto action describing strings propagating in AdS$_4$. As such, minimal surfaces correspond to solutions of a Euclidean non-linear sigma model (NLSM) in a symmetric space that can be reduced to an integrable Hamiltonian system through Pohlmeyer reduction.

The oldest known reduction of this kind is the correspondence of the O(3) NLSM to the sine-Gordon equation [16,17], which is now known to be generalizable to sigma models defined on any symmetric space, such as O(N) [18,19] and CP(N) [20] sigma models. Although Pohlmeyer reduction incorporates a non-local connection between the degrees of freedom of the initial sigma model and the reduced integrable system, it can be shown that the dynamics of the reduced system emerge from a local, systematically derivable Lagrangian density [21–24]. Pohlmeyer reduction has been extended to sigma models describing strings propagating in symmetric spacetime geometries [25–27], including spacetimes particularly interesting in the context of holography, such as AdS$_5 \times$ S^5 [28–30] or AdS$_4 \times$CP^3 [31].

Although the integrability of the reduced system can be used to derive several of its solutions, the non-locality of the relation between the original and the reduced degrees of freedom incommodes the inversion of the reduction and thus, the use of Pohlmeyer reduction for the discovery of solutions of the original sigma model. In the recent literature, a method has been developed for the inversion of Pohlmeyer reduction in the specific case of elliptic solutions of the reduced system, leading to the construction of a class of classical string solutions in AdS$_3$ and dS$_3$ [32]. This class of string solutions includes the known family of spiky string solutions in AdS$_3$ [33], as well as several new ones. In this paper, we exploit these techniques to construct new static minimal surfaces in AdS$_4$, corresponding to elliptic solutions of the reduced system.

In Sect. 2, we review the Pohlmeyer reduction of minimal surfaces in AdS$_4$, as well as the limits of the reduced integrable system for planar and static minimal surfaces. In Sect. 3, we study the elliptic solutions of the reduced system, the emergence of effective Schrödinger problems in the process of inverting Pohlmeyer reduction and the construction of the minimal surfaces adopting the techniques of [32]. In Sect. 4, we study basic properties of the derived minimal surfaces, interesting limits of them, as well as their area and consequently the corresponding entanglement entropy. In Sect. 5, we study the global stability of the elliptic minimal surfaces and possible geometric phase transitions between them. Finally, there is an appendix including useful properties of Weierstrass functions that are used throughout the text.

2 Polhmayer reduction of minimal surfaces in AdS$_4$

Pohlmeyer reduction relates in a non-local way the action of a NLSM defined in a symmetric target space to integrable systems of the family of the sine-Gordon equation. In this section, following the literature [27,31,32], we review the Pohlmeyer reduction of space-like minimal surfaces in AdS$_4$, resulting in a two-component integrable system, which in the specific case of static minimal surfaces it is reduced to the cosh-Gordon equation.

Pohlmeyer reduction of NLSMs defined on a symmetric target space is based on the study of the embedding of the two-dimensional NLSM solution into the symmetric target space, which is in turn embedded into an enhanced higher-dimensional flat space. The AdS$_4$ can be implemented as a submanifold in an enhanced five-dimensional flat space with an extra time-like dimension, i.e. $\mathbb{R}^{(2,3)}$. We denote the coordinates in this enhanced space as Y^{-1}, Y^0, Y^1, Y^2 and Y^3. Then AdS$_4$ is the submanifold

$$Y \cdot Y = -\Lambda^2. \tag{2.1}$$

Furthermore, in the following we will use the notation

$$A^\mu B_\mu \equiv A \cdot B, \tag{2.2}$$

where $g_{\mu\nu} = \text{diag}\{-1, -1, +1, +1, +1\}$.

2.1 Action, equations of motion and Virasoro conditions

A two-dimensional surface in AdS$_4$ can be parametrized with two space-like parameters σ_1 and σ_2. Introducing an auxiliary metric γ, the area that can be written in the form of a Polyakov action as

$$A = \frac{1}{2} \int d\sigma_1 d\sigma_2 \sqrt{\gamma} (\gamma^{ab} \partial_a Y \cdot \partial_b Y + \lambda (Y \cdot Y + \Lambda^2)). \tag{2.3}$$

Selecting the conformal gauge $\gamma_{ab} = e^\omega \delta_{ab}$ and introducing the complex coordinate $z = (\sigma_1 + i\sigma_2)/2$, the action is written as

$$A = \int dz d\bar{z} (\partial Y \cdot \bar{\partial} Y + \lambda (Y \cdot Y + \Lambda^2)). \tag{2.4}$$

The equations of motion for the fields Y are

$$\partial \bar{\partial} Y = \lambda Y, \tag{2.5}$$

while the equation of motion for the Lagrange multiplier λ is the geometric constraint (2.1). We can eliminate the Lagrange multiplier λ from the equations of motion of the fields Y (2.5) using the geometric constraint. We find

$$\partial \bar{\partial} Y = \frac{1}{\Lambda^2} (\partial Y \cdot \bar{\partial} Y) Y. \tag{2.6}$$

The stress-energy tensor takes the form

$$T_{zz} = \partial Y \cdot \partial Y, \tag{2.7}$$

$$T_{\bar{z}\bar{z}} = \bar{\partial} Y \cdot \bar{\partial} Y, \tag{2.8}$$

$$T_{z\bar{z}} = 0. \tag{2.9}$$

Thus, the Virasoro constraints take the form

$$\partial Y \cdot \partial Y = 0. \tag{2.10}$$

2.2 The reduced integrable system

We would like to introduce a basis in the enhanced five-dimensional flat space, which includes the vectors Y, ∂Y and $\bar{\partial} Y$. For the purposes of this section, we will name these vectors as v_1, v_2 and v_3 and introduce two more vectors v_4 and v_5 to form the basis in $\mathbb{R}^{(2,3)}$,

$$v_i = \{Y, \partial Y, \bar{\partial} Y, v_4, v_5\}. \tag{2.11}$$

The vectors ∂Y and $\bar{\partial} Y$ span the tangent space of the two-dimensional surface we study. Although Virasoro conditions suggest that they are both null, this is due to the fact that they are actually complex. Since we study a space-like surface, the tangent space contains two space-like directions and consequently real linear combinations of ∂Y and $\bar{\partial} Y$ will be space-like. It follows that one of the vectors v_4 and v_5 has to be space-like and the other time-like, as the basis should contain two time-like and three space-like vectors and furthermore v_1 is time-like as implied by the geometric constraint (2.1). We choose v_4 to be space-like and v_5 to be time-like and we demand that v_4 has constant norm equal to one, v_5 has constant norm equal to minus one and they are both orthogonal to v_1, v_2 and v_3 and to each other,

$$v_4 \cdot v_5 = v_{4/5} \cdot Y = v_{4/5} \cdot \partial Y = v_{4/5} \cdot \bar{\partial} Y = 0, \tag{2.12}$$
$$v_4 \cdot v_4 = 1, \quad v_5 \cdot v_5 = -1. \tag{2.13}$$

We define the reduced field a as

$$e^a := \partial Y \cdot \bar{\partial} Y, \tag{2.14}$$

since $\partial Y \cdot \bar{\partial} Y$ is a positive quantity.

The form of the inner products of the basis vectors implies that a general vector X in the enhanced space can be decomposed in the basis v_i as

$$X = -\frac{1}{\Lambda^2}(X \cdot v_1) v_1 + e^{-a}(X \cdot v_3) v_2 + e^{-a}(X \cdot v_2) v_3$$
$$+ (X \cdot v_4) v_4 - (X \cdot v_5) v_5. \tag{2.15}$$

We would like to decompose the rate of change of the basis vectors with the complex coordinate z in the basis v_i itself. We do so by defining the complex 5×5 matrix A as

$$\partial v_i = A_{ij} v_j. \tag{2.16}$$

By definition we have $\partial v_1 = v_2$, while the equations of motions for the field Y imply that

$$\partial v_3 = \partial \bar{\partial} Y = \frac{1}{\Lambda^2} e^a Y = \frac{1}{\Lambda^2} e^a v_1. \tag{2.17}$$

For the derivative of v_2, in general we have

$$\partial v_2 = \partial^2 Y = a_0 v_1 + a_+ v_1 + a_- v_2 + a_4 v_4 + a_5 v_5, \tag{2.18}$$

The geometric constraint (2.1) upon differentiation yields $\partial Y \cdot Y = 0$, while upon another differentiation and the use of the Virasoro constraints (2.10), we get $\partial^2 Y \cdot Y = 0$. The latter implies that $a_0 = 0$. Differentiation of the Virasoro constraint (2.10) yields $\partial^2 Y \cdot \partial Y = 0$, implying that $a_- = 0$. Finally, differentiating the definition of the reduced field a (2.14) and using the equations of motion and the fact that Y is orthogonal to its derivative, we get $\partial^2 Y \cdot \bar{\partial} Y = \partial a e^a$, implying that $a_+ = \partial a$. Summing up, we have shown that

$$\partial v_2 = \partial a v_2 + a_4 v_4 + a_5 v_5. \tag{2.19}$$

Finally, the orthogonality conditions for the vectors v_4 and v_5 yield their derivatives as follows:

$$v_{4/5} \cdot v_{4/5} = \pm 1 \Rightarrow \partial v_4 \cdot v_4 = \partial v_5 \cdot v_5 = 0,$$
$$v_4 \cdot v_5 = 0 \Rightarrow \partial v_4 \cdot v_5 = -\partial v_5 \cdot v_4 \equiv f,$$
$$v_{4/5} \cdot Y = 0 \Rightarrow \partial v_{4/5} \cdot Y = -v_{4/5} \cdot \partial Y = 0,$$
$$v_{4/5} \cdot \partial Y = 0 \Rightarrow \partial v_{4/5} \cdot \partial Y = -v_{4/5} \cdot \partial^2 Y = \mp a_{4/5},$$
$$v_{4/5} \cdot \bar{\partial} Y = 0 \Rightarrow \partial v_{4/5} \cdot \bar{\partial} Y = -v_{4/5} \cdot \partial \bar{\partial} Y = 0.$$

Putting everything together, the derivatives of v_4 and v_5 are equal to

$$\partial v_4 = -a_4 e^{-a} v_3 - f v_5, \tag{2.20}$$
$$\partial v_5 = a_5 e^{-a} v_3 - f v_4. \tag{2.21}$$

It is important to notice that $\bar{\partial} v_i \neq \bar{A}_{ij} v_j$, since the basis vectors v_2 and v_3 are not real but rather they are complex conjugates of each other. As a result, it is true that

$$\bar{\partial} v_i = \tilde{A}_{ij} v_j, \tag{2.22}$$

where $\tilde{A}$ is the complex conjugate of the matrix that is produced after the interchange of the second and third lines and rows of A. Thus, the matrices A and $\tilde{A}$ are equal to

$$A = \begin{pmatrix} 0 & 1 & 0 & 0 & 0 \\ 0 & \partial a & 0 & a_4 & a_5 \\ \frac{1}{\Lambda^2} e^a & 0 & 0 & 0 & 0 \\ 0 & 0 & -a_4 e^{-a} & 0 & -f \\ 0 & 0 & a_5 e^{-a} & -f & 0 \end{pmatrix}, \tag{2.23}$$

$$\tilde{A} = \begin{pmatrix} 0 & 0 & 1 & 0 & 0 \\ \frac{1}{\Lambda^2} e^a & 0 & 0 & 0 & 0 \\ 0 & 0 & \bar{\partial} a & \bar{a}_4 & \bar{a}_5 \\ 0 & -\bar{a}_4 e^{-a} & 0 & 0 & -\bar{f} \\ 0 & \bar{a}_5 e^{-a} & 0 & -\bar{f} & 0 \end{pmatrix}. \tag{2.24}$$

The above matrices have to obey the compatibility condition

$$\bar{\partial}(A_{ij} e_j) = \partial(\tilde{A}_{ij} e_j)$$
$$\Rightarrow (\bar{\partial} A_{ij}) e_j + A_{ik} \tilde{A}_{kj} e_j = (\partial \tilde{A}_{ij}) e_j + \tilde{A}_{ik} A_{kj} e_j, \tag{2.25}$$

which in matrix form can be written as the zero-curvature condition

$$\bar{\partial} A - \partial \tilde{A} + [A, \tilde{A}] = 0. \tag{2.26}$$

It is a matter of algebra to show that the zero-curvature condition implies the equations

$$\partial \bar{\partial} a = (|a_4|^2 - |a_5|^2) e^{-a} + \frac{1}{\Lambda^2} e^a, \tag{2.27}$$

$$\partial \bar{f} - \bar{\partial} f = e^{-a} (a_4 \bar{a}_5 - \bar{a}_4 a_5), \tag{2.28}$$

$$\bar{\partial} a_4 = a_5 \bar{f}, \tag{2.29}$$

$$\bar{\partial} a_5 = a_4 \bar{f}. \tag{2.30}$$

Equations (2.29) and (2.30) yield

$$\bar{\partial}(a_4^2 - a_5^2) = 0, \tag{2.31}$$

which allows for the following two inequivalent parametrizations of a_4 and a_5:

$$a_4 = g(z) \cosh \theta(z, \bar{z}), \quad \text{or} \quad a_4 = g(z) \sinh \theta(z, \bar{z}),$$
$$a_5 = g(z) \sinh \theta(z, \bar{z}), \quad\quad a_5 = g(z) \cosh \theta(z, \bar{z}). \tag{2.32}$$

The relative magnitude of a_4 and a_5 determines which parametrization is appropriate. In both cases,

$$\bar{f} = \frac{\bar{\partial} a_4}{a_5} = \bar{\partial} \theta. \tag{2.33}$$

Then Eqs. (2.27) and (2.28) take the form

$$\partial a = \pm |g(z)|^2 \cosh \left(\theta - \bar{\theta}\right) e^{-a} + \frac{1}{\Lambda^2} e^a, \tag{2.34}$$

$$\partial \bar{\partial} \left(\theta - \bar{\theta}\right) = \mp g(z) \bar{g}(\bar{z}) \sinh \left(\theta - \bar{\theta}\right) e^{-a}, \tag{2.35}$$

where the sign depends on the relative magnitude of a_4 and a_5. We define the fields α and β as

$$\alpha := a - \ln \left(\Lambda |g(z)|\right), \tag{2.36}$$

$$\beta := \frac{1}{2} \text{Im} \theta, \tag{2.37}$$

and furthermore we define the complex coordinate $z' = z'(z)$ so that

$$\frac{dz'}{dz} = \sqrt{\Lambda g(z)}. \tag{2.38}$$

Then the reduced equations take the form

$$\partial \bar{\partial} \alpha = \frac{1}{\Lambda^2} \left(\pm \cos \beta e^{-\alpha} + e^{\alpha}\right), \tag{2.39}$$

$$\partial \bar{\partial} \beta = \mp \frac{1}{\Lambda^2} \sin \beta e^{-\alpha}. \tag{2.40}$$

The above equations are derivable from the Lagrangian density

$$\mathscr{L} = \frac{1}{2} \partial \alpha \bar{\partial} \alpha - \frac{1}{2} \partial \beta \bar{\partial} \beta + \frac{1}{\Lambda^2} \left(\mp \cos \beta e^{-\alpha} + e^{\alpha}\right). \tag{2.41}$$

Finally, none of the above parametrizations can describe the special case, where a_4 and a_5 have the same magnitude. In this case, we should parametrize a_4 and a_5 as

$$a_4 = g(z) e^{i\beta(z, \bar{z})}, \tag{2.42}$$

$$a_5 = g(z) e^{-i\beta(z, \bar{z})} \tag{2.43}$$

and it is straightforward to show that Eqs. (2.27) and (2.28) can directly be written as

$$\partial \bar{\partial} \alpha = \frac{1}{\Lambda^2} e^a, \tag{2.44}$$

$$\partial \bar{\partial} \beta = 0, \tag{2.45}$$

which are derivable from the Lagrangian density

$$\mathscr{L} = \frac{1}{2} \partial \alpha \bar{\partial} \alpha - \frac{1}{2} \partial \beta \bar{\partial} \beta + \frac{1}{\Lambda^2} e^\alpha. \tag{2.46}$$

2.3 The area of the minimal surface in the reduced problem

The area of the minimal surface is given by the action (2.4), as the integral of the conformal factor e^a.

$$A = \int dz d\bar{z} e^a. \tag{2.47}$$

However, the reduced integrable system equations are expressed in terms of the fields α and β defined in Eqs. (2.36) and (2.37) and the coordinate z' defined in (2.38). We are interested in acquiring a simple expression for the area of the minimal surface, in terms of the reduced degrees of freedom to facilitate the calculation of the area of the constructed minimal surfaces later. It turns out that the redefinitions (2.36)–(2.38) are nothing more than a conformal transformation, thus, they leave the expression for the area invariant,

$$A = \int dz d\bar{z} e^a$$
$$= \int \frac{dz'}{\sqrt{\Lambda f(z)}} \frac{d\bar{z}'}{\sqrt{\Lambda g(\bar{z})}} \Lambda \sqrt{f(z) g(\bar{z})} e^\alpha \tag{2.48}$$
$$= \int dz' d\bar{z}' e^\alpha.$$

Defining the real and imaginary parts of the complex number z' as $z' = (u + iv)/2$, the area formula takes the form

$$A = \frac{1}{2} \int du dv e^\alpha. \tag{2.49}$$

2.4 Restricting to AdS$_3$ or H^3

We may restrict our attention to "flat" space-like surfaces constrained in the $Y_3 = 0$ plane, i.e. minimal surfaces in AdS$_3$. Such surfaces correspond to $a_4 = 0$ implying that $a_5 = g(z)$. After the appropriate redefinition of the fields and the complex coordinate, we result in the equation

$$\partial\bar{\partial}\alpha = \frac{2}{\Lambda^2}\sinh\alpha, \tag{2.50}$$

which is the Euclidean sinh-Gordon equation.

Similarly, we may restrict our attention to static surfaces in AdS$_4$, i.e. minimal surfaces in the hyperboloid H^3. In this case, we have $a_5 = 0$ implying that $a_4 = g(z)$ yielding the equation

$$\partial\bar{\partial}\alpha = \frac{2}{\Lambda^2}\cosh\alpha, \tag{2.51}$$

which is the Euclidean cosh-Gordon equation.

For both "flat" and static minimal surfaces, the special case $g(z) = 0$ results in the Euclidean Liouville equation

$$\partial\bar{\partial}\alpha = \frac{1}{\Lambda^2}e^\alpha. \tag{2.52}$$

3 Static elliptic minimal surfaces

In this section, we restrict our attention to static minimal surfaces in AdS$_4$, which are mapped through Pohlmeyer reduction to solutions of Eq. (2.51), namely the Euclidean cosh-Gordon equation, as shown in Sect. 2. Furthermore, we focus on a specific class of solutions of the cosh-Gordon equation, having the property that they depend on either the real or the imaginary part of the complex coordinate. It turns out that such solutions can be expressed in terms of elliptic functions. For these elliptic solutions, it is possible to invert Pohlmeyer reduction and find analytic expressions for the corresponding minimal surfaces. The derivation closely follows [32], which applies similar techniques for the construction of classical string solutions, so the reader is encouraged to recur there for more details.

It has to be noticed that it is not possible to find nontrivial solutions of the reduced system with the use of Bäcklund transformations. Although the cosh-Gordon equation possesses Bäcklund transformations similar to those of the sinh-Gordon, it lacks a vacuum solution to serve as the seed solution.

3.1 Elliptic solutions of the cosh-Gordon equation

The Pohlmeyer reduced system equation of interest (2.51), i.e. the Euclidean cosh-Gordon equation can be expressed in terms of the real and imaginary parts of the complex coordinate $z' = (u + iv)/2$ as

$$\frac{\partial^2\alpha}{\partial u^2} + \frac{\partial^2\alpha}{\partial v^2} = \frac{2}{\Lambda^2}\cosh\alpha. \tag{3.1}$$

We restrict our attention to solutions of (3.1) that depend solely on either u or v. Without loss of generality, we assume that they depend on u,

$$\alpha(u, v) = \alpha(u). \tag{3.2}$$

Then the Euclidean cosh-Gordon equation reduces to the following ordinary differential equation:

$$\frac{d^2\alpha}{du^2} = \frac{2}{\Lambda^2}\cosh\alpha, \tag{3.3}$$

which can easily be integrated once to yield

$$\frac{1}{2}\left(\frac{d\alpha}{du}\right)^2 - \frac{2}{\Lambda^2}\sinh\alpha = E. \tag{3.4}$$

Defining

$$e^\alpha = 2\Lambda^2\left(y - \frac{E}{6}\right), \tag{3.5}$$

Equation (3.4) takes the form

$$\left(\frac{dy}{du}\right)^2 = 4y^3 - \left(\frac{E^2}{3} + \frac{1}{\Lambda^4}\right)y + \frac{E}{3}\left(\frac{E^2}{9} + \frac{1}{2\Lambda^4}\right), \tag{3.6}$$

which is the standard form of the Weierstrass equation

$$\left(\frac{dy}{dz}\right)^2 = 4y^3 - g_2 y - g_3, \tag{3.7}$$

where the moduli g_2 and g_3 take the values

$$g_2 = \frac{E^2}{3} + \frac{1}{\Lambda^4}, \tag{3.8}$$

$$g_3 = -\frac{E}{3}\left(\frac{E^2}{9} + \frac{1}{2\Lambda^4}\right). \tag{3.9}$$

In the complex domain, Eq. (3.7) is solved by the Weierstrass elliptic function $\wp(z; g_2, g_3)$. Several of its properties depend on the reality of the roots $e_{1,2,3}$ of the polynomial

$$Q(z) = 4z^3 - g_2 z - g_3. \tag{3.10}$$

In our case, g_2 and g_3 are not arbitrary, but they are given by the expressions (3.8) and (3.9), which imply that all three roots are real independently of the value of the integration constant E. It turns out that the roots are given by simple expressions, which read

$$e_1 = -\frac{E}{12} + \frac{1}{4}\sqrt{E^2 + \frac{4}{\Lambda^4}}, \tag{3.11}$$

$$e_2 = \frac{E}{6}, \tag{3.12}$$

$$e_3 = -\frac{E}{12} - \frac{1}{4}\sqrt{E^2 + \frac{4}{\Lambda^4}}. \tag{3.13}$$

The three roots are defined so that $e_1 > e_2 > e_3$.

Since the polynomial (3.10) has three real roots, independently of the value of the constant E, the fundamental periods of Weierstrass elliptic function $\wp(z; g_2, g_3)$ are a real one $2\omega_1$ and a purely imaginary one $2\omega_2$, given by Eq. (A.13).
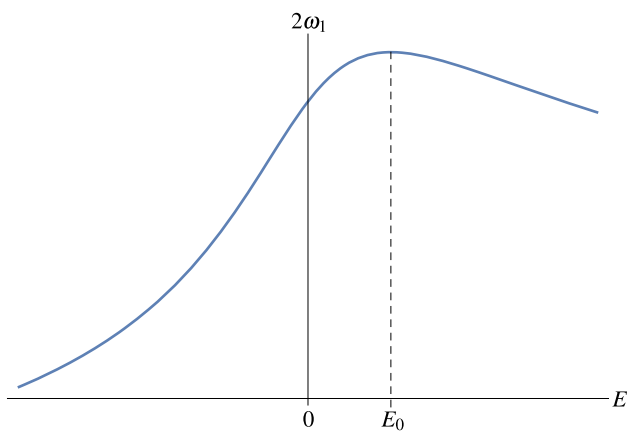
Fig. 1 The period of the elliptic solution as a function of the integration constant E

Furthermore, in this case, Eq. (3.7) has two distinct real solutions in the real domain, namely,

$$y = \wp(x; g_2, g_3), \tag{3.14}$$

$$y = \wp(x + \omega_2; g_2, g_3). \tag{3.15}$$

Both solutions are periodic with period equal to $2\omega_1$. Solution (3.14) ranges from e_1 to infinity, while the second one (3.15) ranges between e_3 and e_2. Equations (3.5) and (3.12) imply that the bounded solution (3.15) does not correspond to a real solution for the reduced field α and consequently, the only acceptable solution for the Pohlmeyer reduced field α that depends solely on variable u is

$$\alpha = \ln[2\Lambda^2(\wp(u; g_2, g_3) - e_2)], \tag{3.16}$$

where g_2 and g_3 are given by Eqs. (3.8) and (3.9) and e_2 is given by Eq. (3.12).

The dependence of the period $2\omega_1$ with the integration constant E is plotted in Fig. 1. There is a global maximum at a positive value of the constant $E = E_0$. In later sections, we will show that the existence of this maximum is related with the stability properties of the elliptic minimal surfaces. Using Eq. (A.3), one can show that E_0 obeys

$$K(k_0) = 2E(k_0), \quad k_0 = \sqrt{\frac{e_2(E_0) - e_3(E_0)}{e_1(E_0) - e_3(E_0)}}, \tag{3.17}$$

resulting in

$$E_0 \simeq 1.72087\Lambda^{-2}. \tag{3.18}$$

One can acquire a qualitative picture for the existence of this maximum. Equation (3.4) can be understood as the energy conservation for an one-dimensional effective mechanical problem of one point particle, where α plays the role of the position coordinate, u plays the role of time, E plays the role of energy and the potential is given by $V = -(2/\Lambda^2)\sinh\alpha$. All solutions for this problem are scattering solutions coming from and going to plus infinity and

for all of them the "time of flight" $2\omega_1$ is finite due to the exponential fall of the potential at $+\infty$. The flattest region of the potential is the region around $u = 0$ and this is the reason the maximum "time of flight" corresponds to a given positive value of the energy constant. For this energy, the point particle spends a relatively large amount of time with small velocity at the flat region, where it is not violently repelled. For energies smaller than this critical value, it does not reach the flat region, while, for larger energies, the point particle does reach the flat region, but it passes through with a larger velocity and then it gets violently reflected in a region where the potential has a steeper slope, thus spending less time with relatively small velocities.

3.2 The effective Schrödinger problems

Given a solution α of the cosh-Gordon equation, the construction of the minimal surface is a non-trivial procedure, due to the non-local nature of the transformation relating the embedding functions Y^μ with the reduced field α (2.14). Such a construction requires the solution of the equations of motion,

$$\frac{\partial^2 Y^\mu}{\partial u^2} + \frac{\partial^2 Y^\mu}{\partial v^2} = \frac{1}{\Lambda^2}e^\alpha Y^\mu, \tag{3.19}$$

simultaneously taking care that the embedding functions Y^μ obey the geometric and Virasoro constraints

$$Y \cdot Y = -\Lambda^2, \tag{3.20}$$

$$\partial Y \cdot \partial Y = 0. \tag{3.21}$$

In Sect. 3.1, we focused on solutions of the reduced system that depend on only one of the two variables. This choice was not arbitrary; for solutions of this kind, Eq. (3.19) can be solved using separation of variables. Defining

$$Y^\mu(u, v) = U^\mu(u) V^\mu(v) \tag{3.22}$$

and using the explicit form of the elliptic solutions for the reduced field α (3.16), we arrive at four pairs of effective Schrödinger problems with opposite eigenvalues, each pair being of the form

$$-U'' + 2(\wp(u; g_2, g_3) - e_2)U = \kappa U, \tag{3.23}$$

$$-\ddot{V} = -\kappa V, \tag{3.24}$$

where the prime stands for differentiation with respect to u, while the dot stands for differentiation with respect to v. We have dropped the indices μ for simplicity, but in general the eigenvalue κ may have a different value for each component. Actually, each component Y^μ may in general be equal to a linear combination of solutions corresponding to various eigenvalues κ, however, in this work we focus on constructions made of solutions corresponding to a single eigenvalue for each component.

Taking advantage of the geometric constraint, the real and imaginary parts of the Virasoro constraint (3.21) can be written in the form

$$\left(\frac{\partial^2 Y}{\partial u^2} - \frac{\partial^2 Y}{\partial v^2}\right) \cdot Y = 0, \tag{3.25}$$

$$\frac{\partial^2 Y}{\partial u \partial v} \cdot Y = 0, \tag{3.26}$$

which are easier to deal with in the language of the effective Schrödinger problems.

Trivially, the flat potential problem (3.24), for positive eigenvalues $\kappa = \ell^2$, has hyperbolic solutions of the form

$$V(v) = c_1 \cosh \ell v + c_2 \sinh \ell v, \tag{3.27}$$

whereas, for negative eigenvalues $\kappa = -\ell^2$, it has trigonometric solutions of the form

$$V(v) = c_1 \cos \ell v + c_2 \sin \ell v. \tag{3.28}$$

3.3 The $n = 1$ Lamé effective Schrödinger problem

The periodic potentials of the class

$$V(x) = n(n+1)\wp(x), \tag{3.29}$$

are called Lamé potentials. For any integer n, it is possible to analytically find the band structure of the problem and it turns out that it contains up to n finite bands plus an infinite band extending to infinite positive energies.

For the elliptic solutions of the Pohlmeyer reduced problem found in Sect. 3.1, the equations for the embedding functions of the minimal surface take the form of effective Schrödinger problems of the form (3.29) with $n = 1$,

$$-\frac{d^2 y}{dx^2} + 2\wp(x) y = \lambda y. \tag{3.30}$$

It is known that the eigenfunctions of the $n = 1$ Lamé problem are given by

$$y_\pm(x; a) = \frac{\sigma(x \pm a)}{\sigma(x)\sigma(\pm a)} e^{-\zeta(\pm\alpha)x} \tag{3.31}$$

with eigenvalues

$$\lambda = -\wp(a). \tag{3.32}$$

These eigenfunctions are linearly independent, as long as the modulus a does not coincide with any of the half-periods of the Weierstrass function appearing in the potential, and, thus, they provide the general solution of the problem. In the degenerate case, both solutions tend to

$$y_\pm(x; \omega_{1,2,3}) = \sqrt{\wp(x) - e_{1,3,2}}, \tag{3.33}$$

where $\omega_3 = \omega_1 + \omega_2$ and there is another linearly independent solution,

$$\tilde{y}(x; \omega_{1,2,3}) = \sqrt{\wp(x) - e_{1,3,2}}(\zeta(x + \omega_{1,2,3}) + e_{1,3,2}x). \tag{3.34}$$

The special functions $\zeta(z)$ and $\sigma(z)$ appearing in the formulas above are the Weierstrass zeta and sigma functions, respectively, which are defined as

$$\frac{d\zeta}{dz} = -\wp, \quad \frac{1}{\sigma}\frac{d\sigma}{dz} = \zeta. \tag{3.35}$$

The functions ζ and σ, unlike the elliptic function $\wp$, are not periodic. More information is provided in the appendix.

It can be shown that the band structure of the $n = 1$ Lamé potential is directly connected with the roots of the cubic polynomial associated with the Weierstrass function appearing in the potential. In the case there are three real roots, which is the case of interest in this study, there is a finite "valence" band for $-e_1 < \lambda < -e_2$ and an infinite "conduction" band for $\lambda > -e_3$. The eigenfunctions $y_\pm$ for eigenvalues within the bands are complex conjugate to each other and upon a shift of their argument by the period $2\omega_1$ they acquire a complex phase as expected by Bloch's theorem. On the contrary, for eigenvalues within the gaps of the spectrum, they are both real and upon a shift of their argument by the period $2\omega_1$ they get multiplied by a real number, in general different from 1, and consequently they diverge exponentially at either plus or minus infinity. Exceptionally, the eigenfunctions (3.33) corresponding to the boundaries of the bands are both real and periodic. These eigenfunctions do not have the physical interpretation of a wavefunction and consequently they do not have to obey any specific normalization conditions. As a result none of them is excluded.

The eigenfunctions (3.31) obey a set of properties that will become useful later,

$$y_+ y_- = \wp(x) - \wp(a), \tag{3.36}$$

$$y_+' y_- - y_+ y_-' = -\wp'(a). \tag{3.37}$$

3.4 Construction of elliptic minimal surfaces

At this point, there is only one step left to complete the inversion of Pohlmeyer reduction for elliptic solutions of the cosh-Gordon equation. The equations of motion are satisfied by the solutions of the effective Schrödinger problems, but one needs to make an appropriate arrangement of such solutions in the components of the embedding functions, so that the geometric and Virasoro constraints are also satisfied.

Since we are constrained to static minimal surfaces, we may select to set $Y^0 = 0$. In the following, we neglect the Y^0 component when we express Y in a matrix form.

Similarly to the construction of classical string solutions in [32], one can show that it is not possible to construct a

minimal surface using solutions of the effective Schrödinger problems corresponding to a single eigenvalue. It turns out that the simplest possible construction involves at least two distinct eigenvalues. The form of the metric of the enhanced space suggests that these eigenvalues should be selected to have opposite signs. Let these eigenvalues be equal to

$$\kappa_1 = \ell_1^2 = -\wp(a_1) - 2e_2, \tag{3.38}$$

$$\kappa_2 = -\ell_2^2 = -\wp(a_2) - 2e_2, \tag{3.39}$$

where a_1 and a_2 are the moduli appearing in the corresponding solutions of the $n = 1$ Lamé effective Schrödinger problem. The form of the eigenvalues restricts a_1 and a_2 so that

$$\wp(a_2) > \wp(a_1). \tag{3.40}$$

The form of the enhanced metric and the geometric and Virasoro constraints favor an ansatz of the form

$$Y = \begin{pmatrix} c_1^+ U_1^+(u)\cosh\ell_1 v + c_1^- U_1^-(u)\sinh\ell_1 v \\ c_1^+ U_1^+(u)\sinh\ell_1 v + c_1^- U_1^-(u)\cosh\ell_1 v \\ c_2^+ U_2^+(u)\cos\ell_2 v + c_2^- U_2^-(u)\sin\ell_2 v \\ c_2^+ U_2^+(u)\sin\ell_2 v - c_2^- U_2^-(u)\cos\ell_2 v \end{pmatrix}, \tag{3.41}$$

where $U_1^\pm(u)$ and $U_2^\pm(u)$ are in general linear combinations of the eigenfunctions of the $n = 1$ Lamé problem, $y_\pm(u; a_1)$ and $y_\pm(u; a_2)$, respectively. The geometric and Virasoro constraints (3.20), (3.25) and (3.26) take the form

$$-\left(c_1^+ U_1^+\right)^2 + \left(c_1^- U_1^-\right)^2 + \left(c_2^+ U_2^+\right)^2 + \left(c_2^- U_2^-\right)^2 = -\Lambda^2, \tag{3.42}$$

$$-\left[-\left(c_1^+ U_1^+\right)^2 + \left(c_1^- U_1^-\right)^2\right]\ell_1^2$$
$$+\left[\left(c_2^+ U_2^+\right)^2 + \left(c_2^- U_2^-\right)^2\right]\ell_2^2 = (\wp(u) - e_2)\Lambda^2, \tag{3.43}$$

$$c_1^+ c_1^-\left(U_1^{+'}U_1^- - U_1^{-'}U_1^+\right)\ell_1$$
$$-c_2^+ c_2^-\left(U_2^{+'}U_2^- - U_2^{-'}U_2^+\right)\ell_2 = 0. \tag{3.44}$$

The geometric constraint (3.42), combined with property (3.36) of the $n = 1$ Lamé eigenfunctions suggests that we have to select

$$c_1^+ = c_1^-,$$
$$U_1^+(u) = \frac{1}{2}\left(y_+(u; a_1) + y_-(u; a_1)\right),$$
$$U_1^-(u) = \frac{1}{2}\left(y_+(u; a_1) - y_-(u; a_1)\right), \tag{3.45}$$
$$c_2^+ = c_2^-,$$
$$U_2^+(u) = \frac{1}{2}\left(y_+(u; a_2) + y_-(u; a_2)\right),$$
$$U_2^-(u) = \frac{1}{2i}\left(y_+(u; a_2) - y_-(u; a_2)\right). \tag{3.46}$$

Reality of the solution directly implies that $y_\pm(u; a_1)$ are non-normalizable eigenstates corresponding to the gaps of the Lamé spectrum, whereas $y_\pm(u; a_2)$ are Bloch waves,

lying within the allowed bands of the Lamé spectrum. Since $\wp(a_1) < \wp(a_2)$, they necessarily lie within the finite gap and in the finite "valence" band of the Lamé spectrum, respectively. Consequently,

$$e_3 < \wp(a_1) < e_2 \quad \text{and} \quad e_2 < \wp(a_2) < e_1. \tag{3.47}$$

Inserting the above selections into the geometric constraint (3.42) yields the equation

$$(-c_1^2 + c_2^2)\wp(u) + (c_1^2\wp(a_1) - c_2^2\wp(a_2)) = -\Lambda^2, \tag{3.48}$$

which in turn implies that

$$c_1^2 = c_2^2 \equiv c^2 = \frac{\Lambda^2}{\wp(a_2) - \wp(a_1)}. \tag{3.49}$$

After some algebra, the Virasoro constraint (3.43) yields

$$\wp(a_1) + \wp(a_2) = -e_2, \tag{3.50}$$

while the Virasoro constraint (3.44), using property (3.37) takes the form

$$\wp'(a_1)\ell_1 = i\wp'(a_2)\ell_2. \tag{3.51}$$

The last equation is always satisfied, as long as (3.50) is satisfied. To verify this, one can make use of Weierstrass equation to rewrite (3.51) as

$$4\left(\wp(a_1) + 2e_2\right)\left(\wp(a_1) - e_1\right)$$
$$\times\left(\wp(a_1) - e_2\right)\left(\wp(a_1) - e_3\right)$$
$$= 4\left(\wp(a_2) + 2e_2\right)\left(\wp(a_2) - e_1\right)$$
$$\times\left(\wp(a_2) - e_2\right)\left(\wp(a_2) - e_3\right). \tag{3.52}$$

Then Eq. (3.50) connects the factors of the left and right hand sides one by one.

Putting everything together, the construction of a minimal surface solution, built from eigenstates of the effective Schrödinger problems corresponding to two distinct eigenvalues, is equivalent to the specification of $\wp(a_1)$ and $\wp(a_2)$ so that obey (3.47), (3.50) and simultaneously are such that the eigenvalues $\kappa_{1,2}$ as specified by (3.38) and (3.39) have the appropriate sign. As shown in Fig. 2, for any value of the integration constant E, there is a set of appropriate selections of $\wp(a_1)$ and $\wp(a_2)$, constituting a linear segment in the $(\wp(a_1), \wp(a_2))$ plane. One of the two endpoints of this linear segment is always (e_3, e_1), while the other one is $(e_2, -2e_2)$ when $E < 0$ and $(-2e_2, e_2)$ when $E > 0$.

The constructed elliptic minimal surfaces are a special case of more general hyperelliptic minimal surfaces studied in the mathematical literature in terms of Riemann theta function [34], as well as in the physics literature in the context of Wilson loops [35,36]. The advantage of our approach is their derivation from a linear problem, resulting in much simpler expressions in terms of Weierstrass elliptic function. These expressions allow an analytic study of their properties,
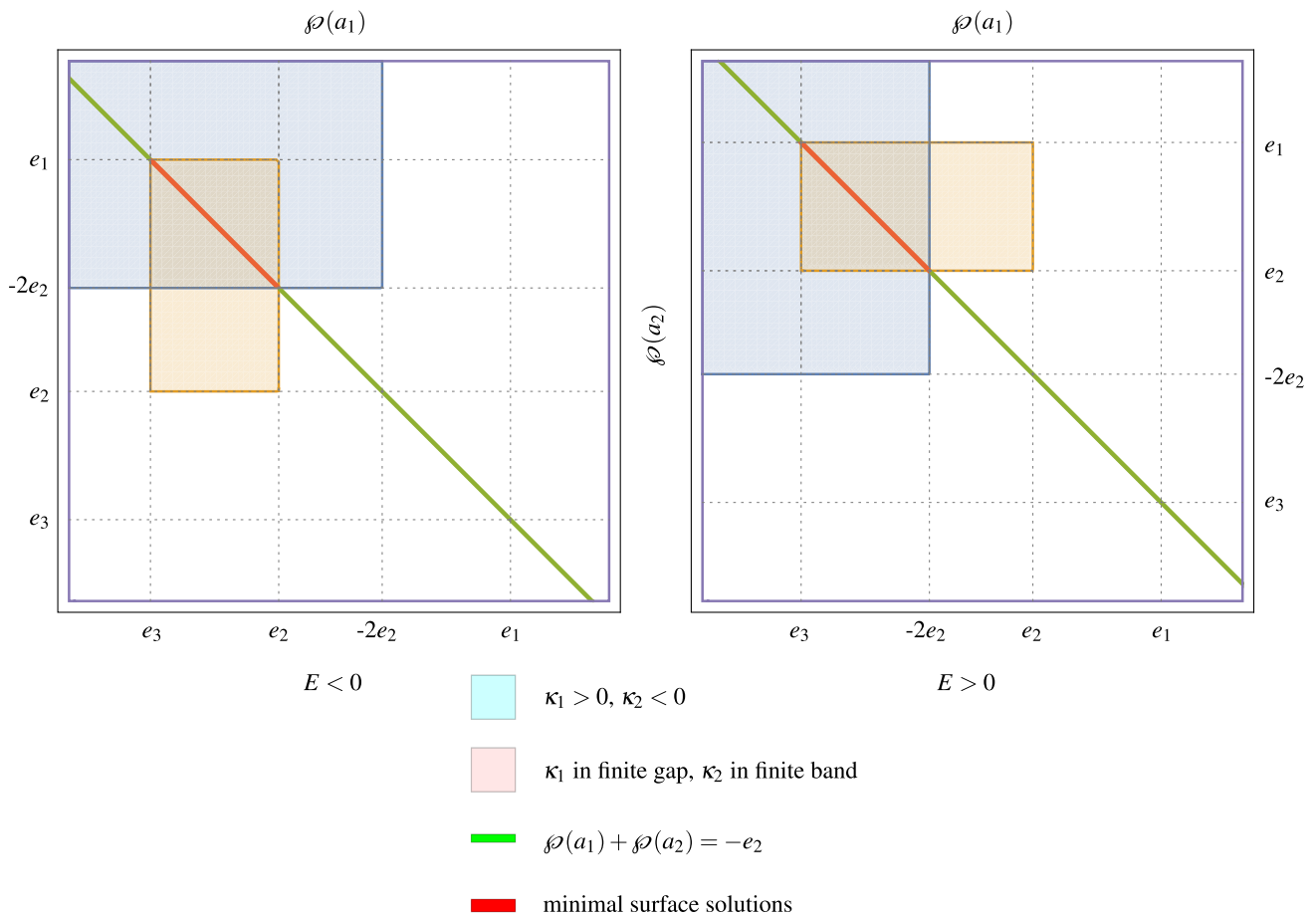
Fig. 2 The pairs of $\wp(a_1)$ and $\wp(a_2)$ that generate minimal surface solutions built from eigenstates of the effective Schrödinger problems corresponding to two distinct eigenvalues

as well as a better understanding of their many-to-one correspondence to solutions of the Pohlmeyer reduced integrable system, namely the cosh-Gordon equation.

4 Properties of the elliptic minimal surfaces

In this section, we study basic geometric properties of the minimal surfaces constructed in Sect. 3.4. We are particularly interesting in the form of their trace at the AdS$_4$ boundary and their area, since in the language of the RT conjecture they play the role of the entangling curve and the corresponding entanglement entropy. Furthermore, we will investigate the specific forms of the minimal surfaces corresponding to the endpoints of the linear segments depicted in Fig. 2 and identify them with well known minimal surfaces in H^3, such as helicoids and catenoids.

4.1 Parameter space of elliptic minimal surfaces

The family of elliptic minimal surfaces that we have constructed contains two free parameters. One of those is the constant of integration E, which alters the moduli of the Weierstrass functions and consequently the roots of the associated cubic polynomial and may take any real value. The other one is the parameter $\wp(a_1)$, which takes values between e_3 and $\min(e_2, -2e_2)$, as shown in Fig. 2. Notice that all minimal surfaces corresponding to the same value of E are mapped to the same solution of the cosh-Gordon equation through Pohlmeyer reduction, independently of the value of $\wp(a_1)$. The space of parameters for the elliptic minimal surfaces is plotted in Fig. 3. The allowed parameters comprise a connected region in the parameter space, bounded by the non-smooth union of three smooth curves. Later on, we will see that these boundary curves correspond to three qualitatively distinct and interesting limits of the solutions.

We may simplify the expressions for the elliptic minimal surfaces that we constructed in Sect. 3.4 taking advantage of the fact that the functions $y_{\pm}(u; a_1)$ are real, whereas the functions $y_{\pm}(u; a_2)$ are complex conjugate to each other. We define

$$y_{\pm}(u; a_1) := r_1(u) e^{\pm \varphi_1(u)}, \tag{4.1}$$

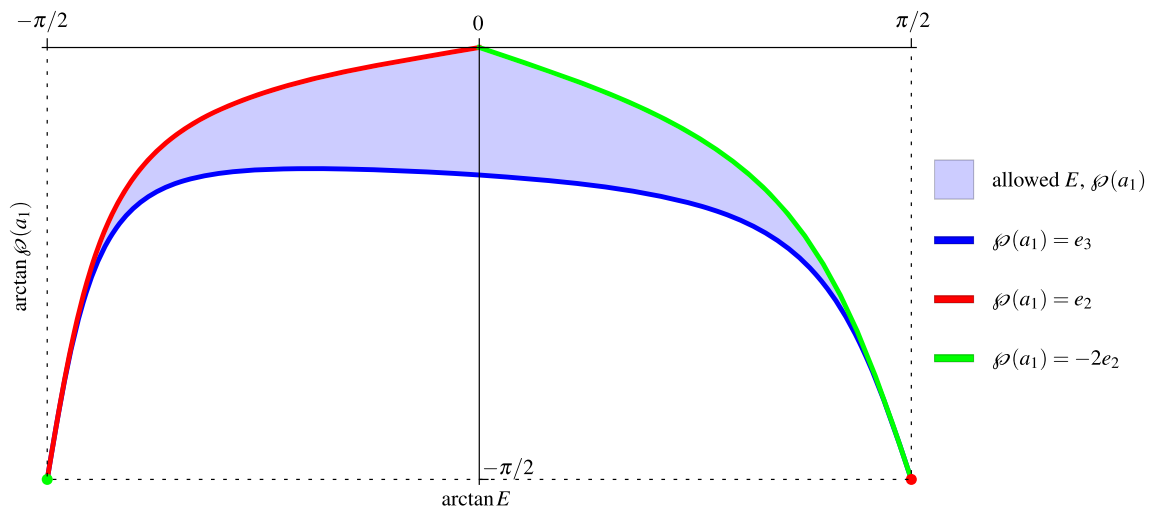$$y_{\pm}(u; a_2) := r_2(u) e^{\pm i \varphi_2(u)}. \tag{4.2}$$

Fig. 3 The parameter space of elliptic minimal surface solutions

A direct application of property (3.36) yields

$$r_1^2(u) = \wp(u) - \wp(a_1), \tag{4.3}$$

$$r_2^2(u) = \wp(u) - \wp(a_2), \tag{4.4}$$

while the explicit form of the $n = 1$ Lamé eigenfunctions (3.31) implies that

$$\varphi_1(u) = \frac{1}{2}\ln\left(-\frac{\sigma(u+a_1)}{\sigma(u-a_1)}\right) - \zeta(a_1)u, \tag{4.5}$$

$$\varphi_2(u) = -\frac{i}{2}\ln\left(-\frac{\sigma(u+a_2)}{\sigma(u-a_2)}\right) + i\zeta(a_2)u. \tag{4.6}$$

Using the above definitions, the minimal surface solution takes the form

$$Y = c\begin{pmatrix} \sqrt{\wp(u) - \wp(a_1)}\cosh(\ell_1 v + \varphi_1(u)) \\ \sqrt{\wp(u) - \wp(a_1)}\sinh(\ell_1 v + \varphi_1(u)) \\ \sqrt{\wp(u) - \wp(a_2)}\cos(\ell_2 v - \varphi_2(u)) \\ \sqrt{\wp(u) - \wp(a_2)}\sin(\ell_2 v - \varphi_2(u)) \end{pmatrix}. \tag{4.7}$$

In order to better visualize the form of the derived minimal surfaces, we will use two common set of coordinates in a constant time slice of AdS$_4$ (i.e. the H^3), the global spherical coordinates (r, θ, φ), defined as

$$Y = \begin{pmatrix} \Lambda\sqrt{1 + \frac{r^2}{\Lambda^2}} \\ r\cos\theta \\ r\sin\theta\cos\varphi \\ r\sin\theta\sin\varphi \end{pmatrix} \tag{4.8}$$

and the Poincaré coordinates (z, r, φ), defined as

$$Y = \begin{pmatrix} \frac{1}{2z}(z^2 + r^2 + \Lambda^2) \\ \frac{1}{2z}(z^2 + r^2 - \Lambda^2) \\ \frac{\Lambda}{z}r\cos\varphi \\ \frac{\Lambda}{z}r\sin\varphi \end{pmatrix}. \tag{4.9}$$

In global coordinates, the metric takes the form

$$ds^2 = \left(1 + \frac{r^2}{\Lambda^2}\right)^{-1}dr^2 + r^2(d\theta^2 + \sin^2\theta d\varphi^2), \tag{4.10}$$

whereas in Poincaré coordinates it takes the form

$$ds^2 = \frac{\Lambda^2}{z^2}(dz^2 + dr^2 + r^2 d\varphi^2). \tag{4.11}$$

In global coordinates, the elliptic minimal surfaces take the parametric form

$$r = \Lambda\sqrt{\frac{\wp(u) - \wp(a_1)}{\wp(a_2) - \wp(a_1)}\cosh^2(\ell_1 v + \varphi_1(u)) - 1}, \tag{4.12}$$

$$\theta = \tan^{-1}\left(\sqrt{\frac{\wp(u) - \wp(a_1)}{\wp(u) - \wp(a_2)}}\mathrm{csch}(\ell_1 v + \varphi_1(u))\right), \tag{4.13}$$

$$\varphi = \ell_2 v - \varphi_2(u). \tag{4.14}$$

It is simple to eliminate v to show that the minimal surface acquires an expression of the form

$$f\left(\varphi - \frac{\ell_2}{\ell_1}\tanh^{-1}\frac{r\cos\theta}{\sqrt{r^2 + \Lambda^2}}, r\sin\theta\right) = 0. \tag{4.15}$$

Similarly, in Poincaré coordinates we arrive at the parametric form

$$z = \Lambda\sqrt{\frac{\wp(a_2) - \wp(a_1)}{\wp(u) - \wp(a_1)}}e^{\ell_1 v + \varphi_1(u)}, \tag{4.16}$$

$$r = \Lambda\sqrt{\frac{\wp(u) - \wp(a_2)}{\wp(u) - \wp(a_1)}}e^{\ell_1 v + \varphi_1(u)}, \tag{4.17}$$

$$\varphi = \ell_2 v - \varphi_2(u). \tag{4.18}$$

Once again, it is trivial to eliminate v to show that the minimal surface is described in closed form as

$$f\left(\varphi - \frac{\ell_2}{\ell_1} \tanh^{-1}\frac{z^2 + r^2 - \Lambda^2}{z^2 + r^2 + \Lambda^2}, \frac{r}{z}\right) = 0. \tag{4.19}$$

Equations (4.12) and (4.16) provide a geometric explanation to the exclusion of the bounded real solution of the Pohlmeyer reduced system. Solutions built on the bounded solution of the reduced problem would not be anchored at the boundary, and, thus, would be compact surfaces shrinkable to a point. As such, they could not be minimal surfaces.

The form of Eqs. (4.15) and (4.19) is not unexpected. The analog of the elliptic minimal surfaces in NLSMs describing string propagation in AdS$_3$ are several classes of solutions, some of them describing rigidly rotating strings, as shown in [32]. Equations (4.15) and (4.19) are the analog of the rigid rotation condition for the elliptic minimal surfaces. It follows that the constructed elliptic minimal surfaces have in general a "helicoid" shape, as shown in Fig. 4. In this figure, as well as in all following figures depicting elliptic minimal surfaces in global coordinates, the plotted radial coordinate is proportional to the tortoise coordinate $r^* = \arctan r$, so that the opaque sphere in the graphs depicts the H^3 boundary.

Furthermore, Fig. 4 indicates that the elliptic minimal surfaces may or may not have self-intersections. Later on, we will specify the condition that the free parameters E and $\wp(a_1)$ must obey in order to generate an embedding minimal surface.

Finally, surfaces characterized by the same integration constant E, apart from having the same counterpart in the Pohlmeyer reduced theory, they comprise an associate (Bonnet) family of minimal surfaces. It is a matter of simple algebra to show that parametrizing the minimal surface with u and v, the first and second fundamental forms acquire the simple expressions

$$\mathrm{I} = \Lambda^2 \left(\wp(u) - e_2\right) \mathrm{diag}\,\{1, 1\}, \tag{4.20}$$

$$\mathrm{II} = \frac{1}{2\Lambda} \mathrm{diag}\,\{1, -1\}. \tag{4.21}$$

The latter imply that the principal curvatures are equal to

$$\kappa_{1,2} = \pm \frac{1}{2\Lambda^3 \left(\wp(u) - e_2\right)}. \tag{4.22}$$

Therefore, the principal curvatures do not depend on the value of $\wp(a_1)$. As a result, changing the value of $\wp(a_1)$ keeping E constant has the effect of a local rotation of the principal curvature directions of the minimal surface.

4.2 The entangling curve

The Ryu–Takayanagi conjecture relates the area of a co-dimension two minimal surface anchored at the boundary of AdS on an entangling surface to the entanglement entropy of
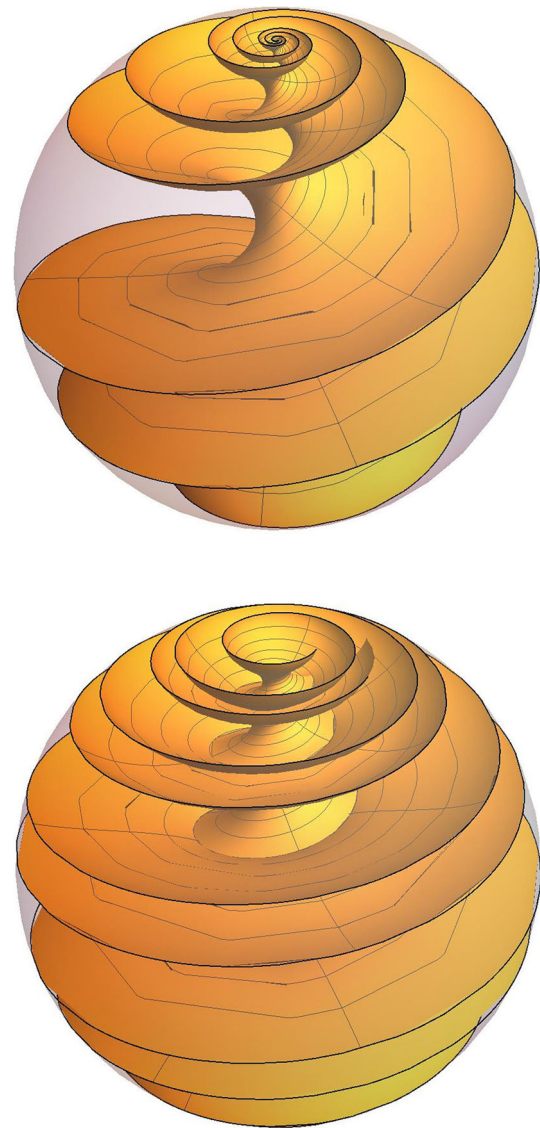

Fig. 4 The elliptic minimal surface in global coordinates for two distinct selections of the parameters E and $\wp(a_1)$

the boundary CFT with respect to the regions separated by the entangling surface (entangling curve in AdS$_4$). Therefore, it is very important to specify what the entangling curve for the constructed elliptical minimal surfaces is.

The minimal surface (4.7) intersects the AdS boundary at the points where the Weierstrass elliptic function diverges, namely $u = 2n\omega_1$. Thus, an appropriately anchored at the boundary minimal surface is spanned by

$$u \in (2n\omega_1, 2(n+1)\omega_1), \quad v \in \mathbb{R}, \tag{4.23}$$

where $n \in \mathbb{Z}$.

The trace of the minimal surfaces on the boundary, i.e. the entangling curve, can be found by taking the limit $u \to 2n\omega_1$. The properties (A.14) and (A.15) of Weierstrass functions imply that

$$\lim_{u \to 2n\omega_1^\pm} y_\pm (u; a) = e^{\pm 2n(\zeta(\omega_1)a - \zeta(a)\omega_1)} \lim_{u \to 0^\pm} \frac{1}{\sigma(u)}. \tag{4.24}$$

Notice that $\sigma(u) = u + \mathcal{O}(u^5)$ and consequently, the limit $\lim_{u \to 2n\omega_1^\pm} y_\pm(u; a)$ depends on whether it is taken from larger or smaller values than $2n\omega_1$. Applying (4.24)–(4.7) yields

$$\lim_{u \to 2n\omega_1^\pm} Y = c \lim_{u \to 0^\pm} \frac{1}{\sigma(u)}$$
$$\times \begin{pmatrix} \cosh(\ell_1 v + 2n(\zeta(\omega_1)a_1 - \zeta(a_1)\omega_1)) \\ \sinh(\ell_1 v + 2n(\zeta(\omega_1)a_1 - \zeta(a_1)\omega_1)) \\ \cos(\ell_2 v + i2n(\zeta(\omega_1)a_2 - \zeta(a_2)\omega_1)) \\ \sin(\ell_2 v + i2n(\zeta(\omega_1)a_2 - \zeta(a_2)\omega_1)) \end{pmatrix}. \tag{4.25}$$

It is convenient to define

$$\delta_1 \equiv \zeta(\omega_1)a_1 - \zeta(a_1)\omega_1, \tag{4.26}$$
$$\delta_2 \equiv \zeta(\omega_1)a_2 - \zeta(a_2)\omega_1. \tag{4.27}$$

The quantities δ_1 and δ_2 have the following properties:

$$\mathrm{Im}\delta_1 = \frac{\pi}{2}, \quad \lim_{\wp(a_1) \to e_3} \mathrm{Re}\delta_1 = 0, \tag{4.28}$$

$$\mathrm{Re}\delta_2 = 0, \quad \lim_{\wp(a_2) \to e_1} \mathrm{Im}\delta_2 = 0, \quad \lim_{\wp(a_2) \to e_2} \mathrm{Im}\delta_2 = \frac{\pi}{2}. \tag{4.29}$$

Denoting as $\theta_\pm(v)$ and $\varphi_\pm(v)$ the angular coordinates of the trace of the extremal surface at the boundary sphere as $u \to 2n\omega_1^+$ and as $u \to 2(n+1)\omega_1^-$, respectively, we find

$$\cot\theta_+ = \pm \sinh(\omega(\varphi_+ + \varphi_0)), \tag{4.30}$$
$$\cot\theta_- = \pm \sinh(\omega(\varphi_- + \varphi_0 - \delta\varphi)), \tag{4.31}$$

where

$$\omega = \frac{\ell_1}{\ell_2}, \tag{4.32}$$

$$\delta\varphi = \pi - 2\left(\mathrm{Im}\delta_2 + \frac{\ell_2}{\ell_1}\mathrm{Re}\delta_1\right). \tag{4.33}$$

Each of these curves have a spiral form and endpoints at the north and south poles of the boundary sphere. As such, one of them cannot split the boundary to two regions, but the union of the two spirals does so.

Similarly, converting to Poincaré coordinates and denoting as $r_\pm(v)$ and $\varphi_\pm(v)$ the polar coordinates of the trace of the extremal surface at the boundary plane as $u \to 2n\omega_1^+$ and as $u \to 2(n+1)\omega_1^-$, respectively, we find

$$r_+ = \Lambda e^{\omega(\varphi_+ + \varphi_0)}, \tag{4.34}$$
$$r_- = \Lambda e^{\omega(\varphi_- + \varphi_0 - \delta\varphi)}. \tag{4.35}$$

So in Poincaré coordinates, the trace of the minimal surface in the boundary is the union of two logarithmic spirals with the same exponential coefficient. The two curves comprising the
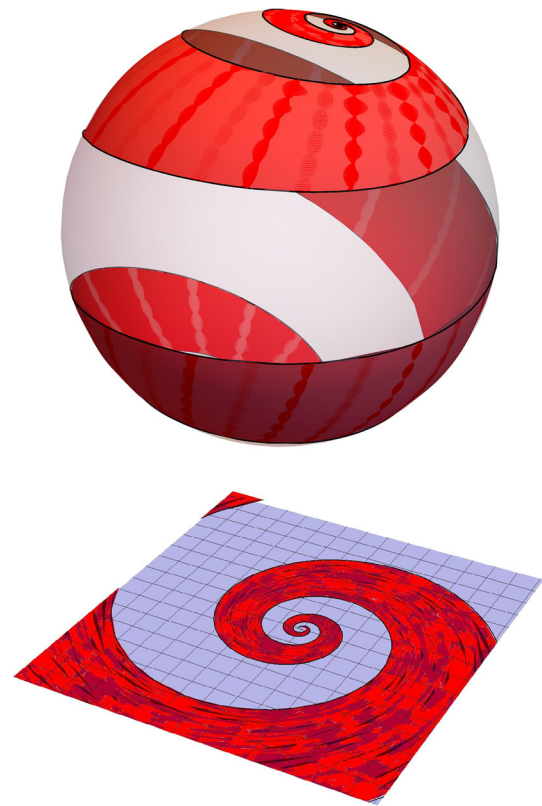

Fig. 5 The entangling curve and the corresponding boundary regions in global and Poincaré coordinates

trace of the minimal surface at the boundary are connected through a rotation of the angle φ by $\delta\varphi$.

In general, the entangling curve separates the boundary to two regions of unequal size. The ratio of the area of two regions is simply $(\delta\varphi \mod 2\pi)/(2\pi - \delta\varphi \mod 2\pi)$. The form of the entangling curve and the corresponding boundary regions in both global and Poincaré coordinates are displayed in Fig. 5.

The entangling curve, which sets the Plateau problem for the minimal surface, is solely determined by the parameters ω and $\delta\varphi$. It is an interesting question whether in the family of elliptic minimal surfaces (4.7), there are different solutions corresponding to the same pair of ω and $\delta\varphi$ and thus to the same entangling curve. (Surfaces corresponding to the same ω and two $\delta\varphi$ that sum to 2π also correspond to the same entangling curve.)

Finally, the parameter $\delta\varphi$ determines whether the minimal surface has self-intersections. Embedding minimal surfaces have the property

$$\delta\varphi < 2\pi. \tag{4.36}$$

For $E > 0$ the parameter ω can become arbitrarily close to zero as $\wp(a_1)$ approaches $-2e_2$. Equation (4.33) implies that at the same limit the angle $\delta\varphi$ becomes arbitrarily large

and consequently larger than 2π. The special case $\omega = 0$ is an exception to this rule as we will show later.

4.3 Area and entanglement entropy

The minimal surface is spanned for u and v taking values in the ranges defined in Eq. (4.23). Consequently, the area of the minimal surface can be directly calculated with the use of formula (2.49),

$$A = \Lambda^2 \int_{-\infty}^{+\infty} dv \int_{2n\omega_1}^{2(n+1)\omega_1} du \, (\wp(u) - e_2). \tag{4.37}$$

The length of the entangling curve, as u and v are isothermal coordinates, can be expressed as

$$L = \lim_{u \to 2n\omega_1^+} \Lambda \int_{-\infty}^{+\infty} dv \sqrt{\wp(u) - e_2}$$
$$+ \lim_{u \to 2(n+1)\omega_1^-} \Lambda \int_{-\infty}^{+\infty} dv \sqrt{\wp(u) - e_2}. \tag{4.38}$$

Straightforward application of Eqs. (A.8) and (A.14) yields

$$A = \Lambda^2 \int_{-\infty}^{+\infty} dv \left(\lim_{u \to 0^+} \zeta(u) - \lim_{u \to 0^-} \zeta(u) \right.$$
$$\left. - 2\zeta(\omega_1) - 2e_2\omega_1 \right) \tag{4.39}$$
$$= 2\Lambda^2 \left(\lim_{u \to 0^+} \frac{1}{u} - \zeta(\omega_1) - e_2\omega_1 \right) \int_{-\infty}^{+\infty} dv,$$

while

$$L = 2\Lambda \int_{-\infty}^{+\infty} dv \lim_{u \to 0^+} \frac{1}{u}. \tag{4.40}$$

Thus, we recover the usual "area law" [37,38], plus a universal constant term,

$$A = \Lambda L - 2\Lambda^2 \left(\zeta(\omega_1) + e_2\omega_1 \right) \int_{-\infty}^{+\infty} dv. \tag{4.41}$$

The universal constant term diverges. In global coordinates the divergence can be attributed to the non-smoothness of the entangling curve at the poles [39]. In Poincaré coordinates, additionally, the entangling curve is infinite, similarly to the case of the minimal surface corresponding to an infinite strip. This divergence introduces a subtlety in the comparison of the areas of two distinct surfaces corresponding to the same entangling curve, as one may rescale v for each of those at will. An appropriate regularization of the universal constant term must enforce that v is connected to the physical position of a given point on the entangling curve. In both sets of coordinates, the azimuthal angle φ, which specifies uniquely a point on the spiral entangling curve, is given by $\varphi = \ell_2 v + \varphi_0$. Consequently, an appropriate redefinition of the parameter v is

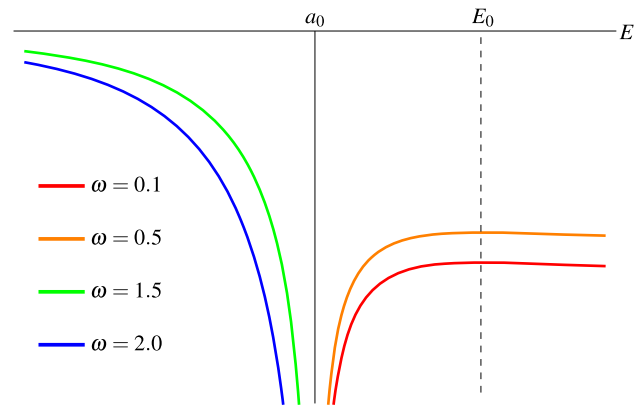$$v = \frac{\varphi}{\ell_2}, \tag{4.42}$$

Fig. 6 The coefficient a_0 as a function of the integration constant E for various ω

leading to

$$A = \Lambda L - \sqrt{2}\Lambda^2 \sqrt{\frac{1 - \omega^2}{E}} \left(\frac{E}{3}\omega_1 + 2\zeta(\omega_1) \right) \int_{-\infty}^{+\infty} d\varphi. \tag{4.43}$$

We define the quantity

$$a_0(E, \omega) := -\sqrt{2}\Lambda^2 \sqrt{\frac{1 - \omega^2}{E}} \left(\frac{E}{3}\omega_1(E) + 2\zeta(\omega_1(E)) \right), \tag{4.44}$$

which can be used as a measure of comparison for the areas corresponding to the same entangling curve. It can be shown that a_0 is always negative, it diverges to minus infinity at $E \to 0$ and

$$\frac{\partial}{\partial E} a_0(E, \omega) < 0, \quad \text{for} \quad E < 0,$$
$$\frac{\partial}{\partial E} a_0(E, \omega) > 0, \quad \text{for} \quad 0 < E < E_0, \tag{4.45}$$
$$\frac{\partial}{\partial E} a_0(E, \omega) < 0, \quad \text{for} \quad E > E_0,$$

where E_0 is the energy constant maximizing the real period of the Weierstrass function, given by Eq. (3.18). Figure 6 depicts the dependence of a_0 on the energy constant E.

4.4 Interesting limits

In Sect. 4.1, we showed that the space of allowed parameters E and $\wp(a_1)$ for elliptic minimal surfaces is bounded by three curves, namely, $\wp(a_1) = e_3(E)$, $\wp(a_1) = e_2(E)$ and $\wp(a_1) = -2e_2(E)$. These curves correspond to interesting limits of the elliptic minimal surfaces.

4.4.1 The helicoid limit

One of the boundaries of the moduli space is $\wp(a_1) = e_3$ and $\wp(a_2) = e_1$, for all values of E. Comparing with the elliptic classical string solutions presented in [32], this special limit is the analog to the Gubser–Klebanov–Polyakov limit [40] of the spiky string solutions.

At these special points of the moduli space, the solution acquires a simpler form. All wavefunctions of the $n = 1$ Lamé problem that appear in the minimal surface solution become simultaneously real and periodic as they correspond to eigenvalues at the edges of the bands of the Lamé spectrum. Consequently, both functions φ_1 and φ_2 vanish identically and the solution acquires the simple form

$$Y = \frac{\Lambda}{\sqrt{e_1 - e_3}} \begin{pmatrix} \sqrt{\wp(u) - e_3} \cosh\left(\sqrt{e_1 - e_2}v\right) \\ \sqrt{\wp(u) - e_3} \sinh\left(\sqrt{e_1 - e_2}v\right) \\ \sqrt{\wp(u) - e_1} \cos\left(\sqrt{e_2 - e_3}v\right) \\ \sqrt{\wp(u) - e_1} \sin\left(\sqrt{e_2 - e_3}v\right) \end{pmatrix},$$

(4.46)

which has the form of a helicoid in H^3. It is not surprising that the minimal surface being the analog of the GKP solution, i.e. a rigidly rotating rod, is a ruled surface.

Converting to global coordinates on the hyperboloid H^3, the helicoid minimal surface take the following parametric form:

$$r = \frac{\Lambda}{\sqrt{e_1 - e_3}} \sqrt{(\wp(u) - e_3)\cosh^2\sqrt{e_1 - e_2}v - (e_1 - e_3)},$$

$$\theta = \tan^{-1}\left(\sqrt{\frac{\wp(u) - e_1}{\wp(u) - e_3}}\operatorname{csch}\sqrt{e_1 - e_2}v\right),$$

$$\varphi = \sqrt{e_2 - e_3}v,$$

(4.47)

which can be written in closed form as

$$r = \Lambda\sqrt{\frac{1}{\cos^2\theta\operatorname{csch}^2\omega\varphi - \sin^2\theta}}.$$

(4.48)

where

$$\omega^2 = \frac{e_1 - e_2}{e_2 - e_3} = \frac{-E + \sqrt{E^2 + 4\Lambda^{-4}}}{E + \sqrt{E^2 + 4\Lambda^{-4}}}.$$

(4.49)

Similarly, in Poincaré coordinates, the helicoid takes the parametric form

$$z = \Lambda\sqrt{\frac{e_1 - e_3}{\wp(u) - e_3}}e^{-\sqrt{e_1 - e_2}v},$$

(4.50)

$$r = \Lambda\sqrt{\frac{\wp(u) - e_1}{\wp(u) - e_3}}e^{-\sqrt{e_1 - e_2}v},$$

(4.51)

$$\varphi = \sqrt{e_2 - e_3}v,$$

(4.52)

which can be written in closed form as

$$z = \sqrt{\Lambda^2 e^{-2\omega\varphi} - r^2}.$$
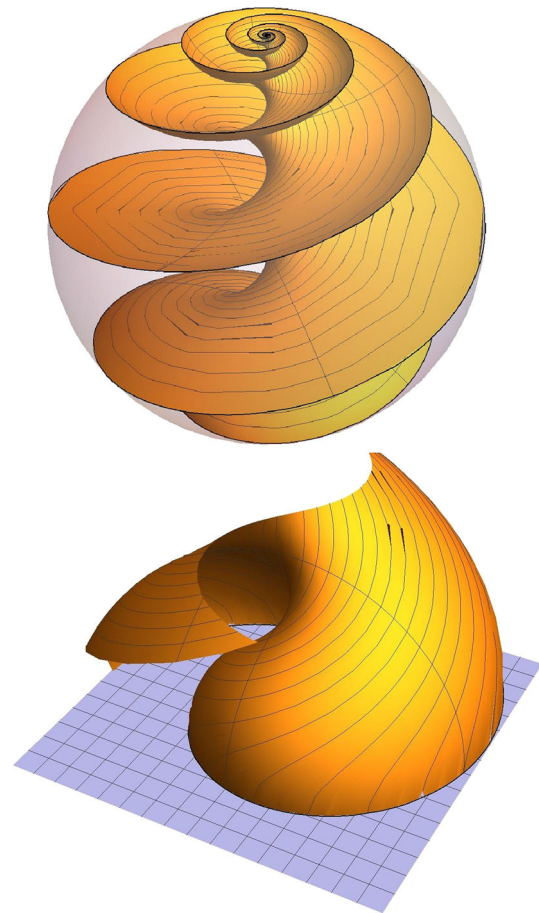
(4.53)

Fig. 7 The helicoid minimal surface in global and Poincaré coordinates

The helicoid minimal surface in both sets of coordinates is depicted in Fig. 7.

As the integration constant E tends to plus infinity, ω tends to zero and the minimal surface becomes the equatorial plane $\theta = \pi/2$ in global coordinates. In Poincaré coordinates, in this limit the logarithmic spiral degenerates to a circle of radius Λ and the minimal surface to the usual "semi-sphere" $z = \sqrt{\Lambda^2 - r^2}$. As the energy constant E tends to minus infinity, ω tends to infinity and the minimal surface tends to the meridian plane $\tan\varphi = \tan\varphi_0$ in global coordinates, while in the Poincaré coordinates the entangling curve degenerates to a straight line passing through the origin and the minimal surface to the infinite semi-plane $\tan\varphi = \tan\varphi_0$.

Finally, the properties (4.28) and (4.29) imply that the parameter $\delta\varphi$ for all helicoid minimal surfaces equals

$$\delta\varphi_{\text{helicoid}} = \pi.$$

(4.54)

Therefore, the entangling curve corresponding to a helicoid minimal surface separates the boundary to two regions of equal area.

4.4.2 The catenoid limit

The second boundary of the moduli space that we are going to consider is $\wp(a_1) = -2e_2$ and $\wp(a_2) = e_2$ for $E > 0$. In this case, only one of the two $n = 1$ Lamé eigenfunctions that appear in the solution corresponds to the edge of a band of the spectrum and thus, it becomes simultaneously periodic and real, allowing the solution to reduce to

$$Y = \frac{\Lambda}{\sqrt{3e_2}} \begin{pmatrix} \sqrt{\wp(u) + 2e_2} \cosh(\varphi_1(u; a_1)) \\ \sqrt{\wp(u) + 2e_2} \sinh(\varphi_1(u; a_1)) \\ \sqrt{\wp(u) - e_2} \cos\left(\sqrt{3e_2}v\right) \\ \sqrt{\wp(u) - e_2} \sin\left(\sqrt{3e_2}v\right) \end{pmatrix}, \quad (4.55)$$

where $\wp(a_1) = -2e_2$.

Although in this case we cannot acquire a closed form for the solution, the shape of the minimal surface can be understood by simple observations. Converting to global coordinates we find

$$r = \frac{\Lambda}{\sqrt{3e_2}} \sqrt{(\wp(u) + 2e_2) \cosh^2 \varphi_1(u; a_1) - 3e_2} = r(u), \quad (4.56)$$

$$\theta = \tan^{-1}\left(\sqrt{\frac{\wp(u) - e_2}{\wp(u) + 2e_2}} \operatorname{csch} \varphi_1(u; a_1)\right) = \theta(u), \quad (4.57)$$

$$\varphi = \sqrt{3e_2}v = \varphi(v). \quad (4.58)$$

Therefore, the surface can be expressed in the form

$$f(r, \theta) = 0 \quad (4.59)$$

and consequently it is a surface of revolution. Since it is both a minimal surface and a surface of revolution, it is by definition a catenoid in H^3. Similarly in Poincaré coordinates, we acquire the expression

$$z = \Lambda \sqrt{\frac{3e_2}{\wp(u) + 2e_2}} e^{-\varphi_1(u; a_1)} = z(u), \quad (4.60)$$

$$r = \Lambda \sqrt{\frac{\wp(u) - e_2}{\wp(u) + 2e_2}} e^{-\varphi_1(u; a_1)} = r(u), \quad (4.61)$$

$$\varphi = \sqrt{3e_2}v = \varphi(v), \quad (4.62)$$

having the same interpretation of a surface by revolution. Figure 8 depicts such a catenoid in global and Poincaré coordinates.

Following the discussion of Sect. 4.2 the parameters ω and $\delta\varphi$ that specify the shape of the entangling curve at the catenoid limit acquire the values

$$\omega_{\text{catenoid}} = 0, \quad (4.63)$$

$$\delta\varphi_{\text{catenoid}} = +\infty. \quad (4.64)$$

As all catenoids are characterized by the same degenerate ω and $\delta\varphi$, the corresponding entangling curve cannot
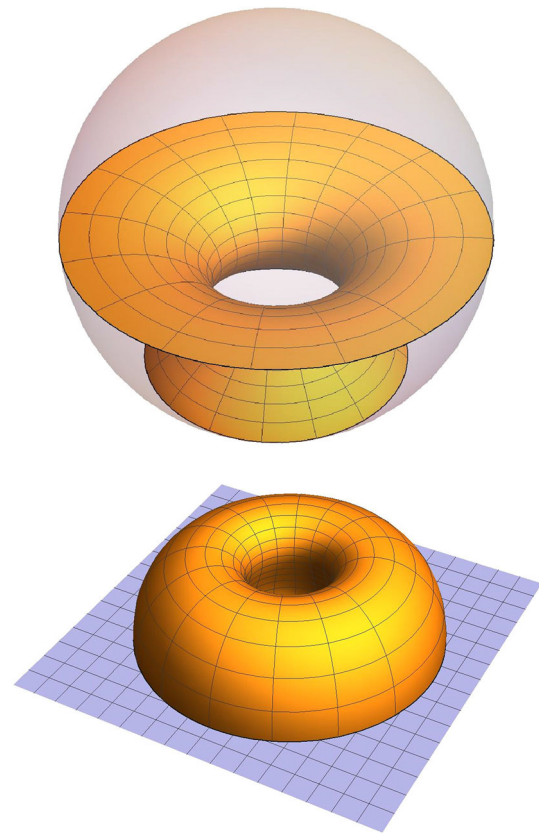

Fig. 8 The catenoid minimal surface in global and Poincaré coordinates

be identified by these parameters for this class of surfaces. The catenoid minimal surface in global coordinates extends between angles

$$\cot\theta_+ = (-1)^n \sinh(2n\operatorname{Re}\delta_1), \quad (4.65)$$

$$\cot\theta_- = (-1)^n \sinh(2(n+1)\operatorname{Re}\delta_1), \quad (4.66)$$

which define two circles parallel to the equator that comprise the entangling curve. In Poincaré coordinates, the entangling curve comprises two concentric circles with radii r_+ and r_-. In the following, the ratio r_-/r_+ is used to characterize the form of the entangling curve in the case of catenoids. This ratio is given by

$$\frac{r_-}{r_+} = e^{2\operatorname{Re}\delta_1} \quad (4.67)$$

and it is plotted versus the integration constant E in Fig. 9.

The ratio r_-/r_+ obeys $\lim_{E \to 0} r_-/r_+ = \lim_{E \to \infty} r_-/r_+ = 1$ and it acquires its minimum value

$$\left(\frac{r_-}{r_+}\right)_0 \simeq 0.367039 \quad (4.68)$$

at $E = E_0$. For ratios $r_-/r_+ > (r_-/r_+)_0$ there are two catenoids anchored at the same entangling curve, whereas for $r_-/r_+ < (r_-/r_+)_0$ there is none.
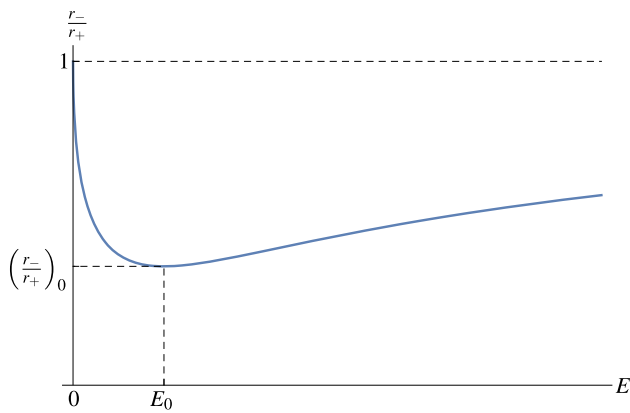
Fig. 9 The ratio of the radii of the circles comprising the entangling curve of a catenoid in Poincaré coordinates, as function of the integration constant E

Unlike the general case, where the parameter v has to take values in the whole real axis in order to span the minimal surface, in the catenoid limit the range of the coordinate v becomes finite and specifically $v \in \left[0, 2\pi/\sqrt{3e_2}\right]$. It is a direct consequence that the universal constant term in the area formula (4.43) becomes finite and specifically,

$$A_{\text{catenoid}} = \Lambda L - 2\pi \Lambda^2 \sqrt{\frac{2}{E}} \left(\frac{E}{3}\omega_1 + 2\zeta(\omega_1)\right). \quad (4.69)$$

In the case of catenoids it is convenient to define the quantity

$$
\begin{aligned}
a_0^{\text{catenoid}}(E) &:= -2\pi \Lambda^2 \sqrt{\frac{2}{E}} \left(\frac{E}{3}\omega_1(E) + 2\zeta(\omega_1(E))\right) \\
&= 2\pi a_0(E, 0), \quad (4.70)
\end{aligned}
$$

which can be used to compare the area of catenoids corresponding the same entangling curve. The quantity a_0^{catenoid} has the same monotonicity properties as a_0.

4.4.3 The conical limit

The last boundary of the moduli space of the elliptic minimal surfaces is $\wp(a_1) = e_2$ and $\wp(a_2) = -2e_2$ for $E < 0$. Similarly to the catenoid limit, only one of the two Lamé eigenfunctions becomes real and periodic and the solution reduces to

$$Y = \frac{\Lambda}{\sqrt{-3e_2}} \begin{pmatrix} \sqrt{\wp(u) - e_2} \cosh\left(\sqrt{-3e_2}v\right) \\ \sqrt{\wp(u) - e_2} \sinh\left(\sqrt{-3e_2}v\right) \\ \sqrt{\wp(u) + 2e_2} \cos(\varphi_2(u; a_2)) \\ -\sqrt{\wp(u) + 2e_2} \sin(\varphi_2(u; a_2)) \end{pmatrix}, \quad (4.71)$$

where $\wp(a_2) = -2e_2$.

Converting to global coordinates, we find

$$r = \frac{\Lambda}{\sqrt{-3e_2}} \sqrt{(\wp(u) - e_2) \cosh^2\left(\sqrt{-3e_2}v\right) + 3e_2}, \quad (4.72)$$

$$\theta = \tan^{-1}\left(\sqrt{\frac{\wp(u) + 2e_2}{\wp(u) - e_2}} \operatorname{csch}\left(\sqrt{-3e_2}v\right)\right), \quad (4.73)$$

$$\varphi = -\varphi_2(u; a_2), \quad (4.74)$$

implying that the specific case of minimal surfaces can be written in the form

$$f(r\sin\theta, \varphi) = 0. \quad (4.75)$$

In Poincaré coordinates we find

$$z = \Lambda \sqrt{\frac{-3e_2}{\wp(u) - e_2}} e^{-\sqrt{-3e_2}v}, \quad (4.76)$$

$$r = \Lambda \sqrt{\frac{\wp(u) + 2e_2}{\wp(u) - e_2}} e^{-\sqrt{-3e_2}v}, \quad (4.77)$$

$$\varphi = \varphi_2(u; a_2), \quad (4.78)$$

implying that the minimal surface can be expressed in the form

$$f\left(\frac{r}{z}, \varphi\right) = 0. \quad (4.79)$$

This expression describes a conical surface with the tip of the cone placed at the origin of the boundary plane. Figure 10 depicts the conical minimal surfaces in global and Poincaré coordinates.

At the limit of the conical minimal surfaces, the parameters ω and $\delta\varphi$, which specify the entangling curve, take the values

$$\omega_{\text{conical}} = \infty, \quad (4.80)$$

$$\delta\varphi_{\text{conical}} = \pi - 2\operatorname{Im}\delta_2. \quad (4.81)$$

In the specific case of the conical minimal surfaces, the area formula (4.43) becomes problematic. The reason is the fact that the azimuthal angle φ is a function solely of u. Thus, the substitution of v with the azimuthal angle φ, performed to introduce an integration variable that is geometrically connected to the points of the entangling curve, unfortunately fails. In this case v is related with the polar angle. An appropriate redefinition is $x = -3e_2v$ and it yields

$$A_{\text{conical}} = \Lambda L + \frac{2}{3}\Lambda^2 \left(\omega_1 + \frac{\zeta(\omega_1)}{e_2}\right) \int_{-\infty}^{+\infty} dx. \quad (4.82)$$

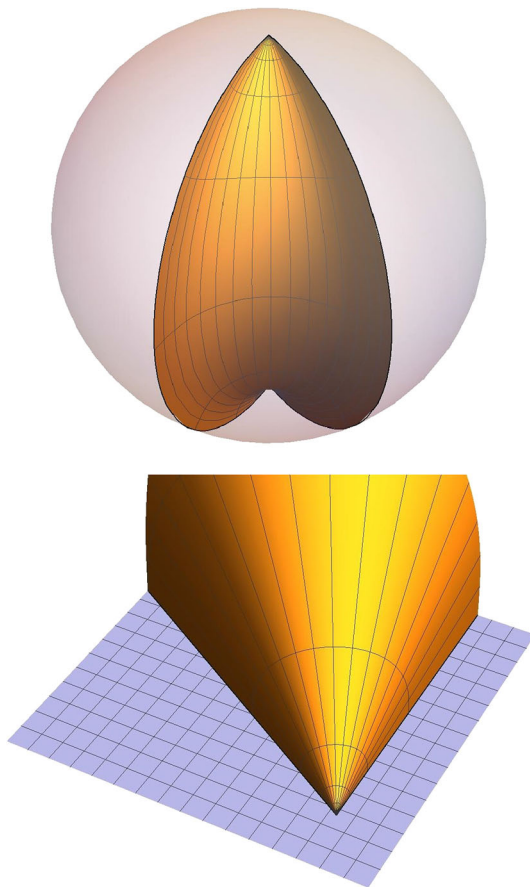The universal term is diverging due to the non-smoothness of the entangling curve.

Fig. 10 The conical minimal surface in global and Poincaré coordinates

5 Geometric phase transitions

5.1 Spiral entangling curves

In general the entangling curve for the elliptic minimal surfaces separates the boundary sphere to two regions. The only exception to this rule is the case of the catenoids, where the entangling curve is the union of two disjoint circles and consequently separates the boundary sphere to three regions. Thus, as long as we do not study catenoid elliptic minimal surfaces, there is no way to find two different minimal surfaces corresponding to the same entangling curve as a result of topological rearrangement of the matching of minimal surfaces and entangling curves.

However, one has to examine whether several of the elliptic minimal surfaces correspond to the same boundary curve. As shown in Sect. 4.2, the boundary curve is determined solely by the parameters ω and $\delta\varphi$. As the dependence of $\delta\varphi$ on the primary parameters E and $\wp(a_1)$ is quite complicated, the simpler way to determine whether there are minimal surfaces with the same entangling curve is plotting $\delta\varphi$ versus the energy constant along constant ω curves in the moduli space of solutions. Such constant ω curves have the form

$$\wp(a_1) = \frac{\omega^2 + 2}{\omega^2 - 1}\frac{E}{6}. \tag{5.1}$$

The constant ω curves for $\omega < 1$ lie entirely in the $E > 0$ region, whereas the parameters $\omega > 1$ lie entirely in the $E < 0$ region. The segment of each constant ω curve within the allowed region of parameters for elliptic minimal surface solutions has one endpoint being a helicoid with $E = E_h(\omega)$, where

$$E_h(\omega) = \frac{1}{\omega} - \omega, \tag{5.2}$$

whereas the other endpoint lies always at $E = \wp(a_1) = 0$.

It can be shown that $\delta\phi$ as a function of E and ω has the following properties:

$$\lim_{E \to 0} \delta\varphi(E, \omega) = 0, \quad \lim_{E \to E_h(\omega)} \delta\varphi(E, \omega) = \pi \tag{5.3}$$

and

$$\frac{\partial}{\partial E}\delta\varphi(E, \omega) < 0, \quad \text{for} \quad E < 0,$$

$$\frac{\partial}{\partial E}\delta\varphi(E, \omega) > 0, \quad \text{for} \quad 0 < E < E_0, \tag{5.4}$$

$$\frac{\partial}{\partial E}\delta\varphi(E, \omega) < 0, \quad \text{for} \quad E > E_0.$$

The above properties are evident in Fig. 11, which depicts the dependence of $\delta\varphi$ on E for various values of ω.

We define the critical value ω_0, for the ω parameter as

$$E_h(\omega_0) = E_0, \tag{5.5}$$

which implies that

$$\omega_0 \simeq 0.458787. \tag{5.6}$$

Notice that $\delta\varphi$ and $2\pi - \delta\varphi$ correspond to the same entangling curve. The above properties of $\delta\varphi(E, \omega)$ imply that for a given entangling curve being characterized by given ω_1 and $\delta\varphi_1 \leq \pi$ there are the following possibilities for an elliptic minimal surface:
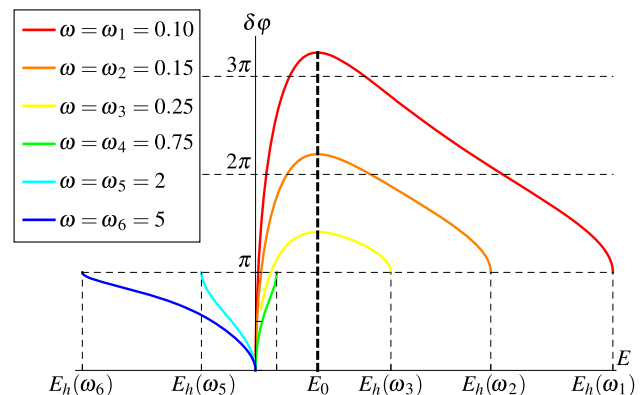

Fig. 11 The dependence of $\delta\varphi$ on the integration constant E along various constant ω curves in the parameter space
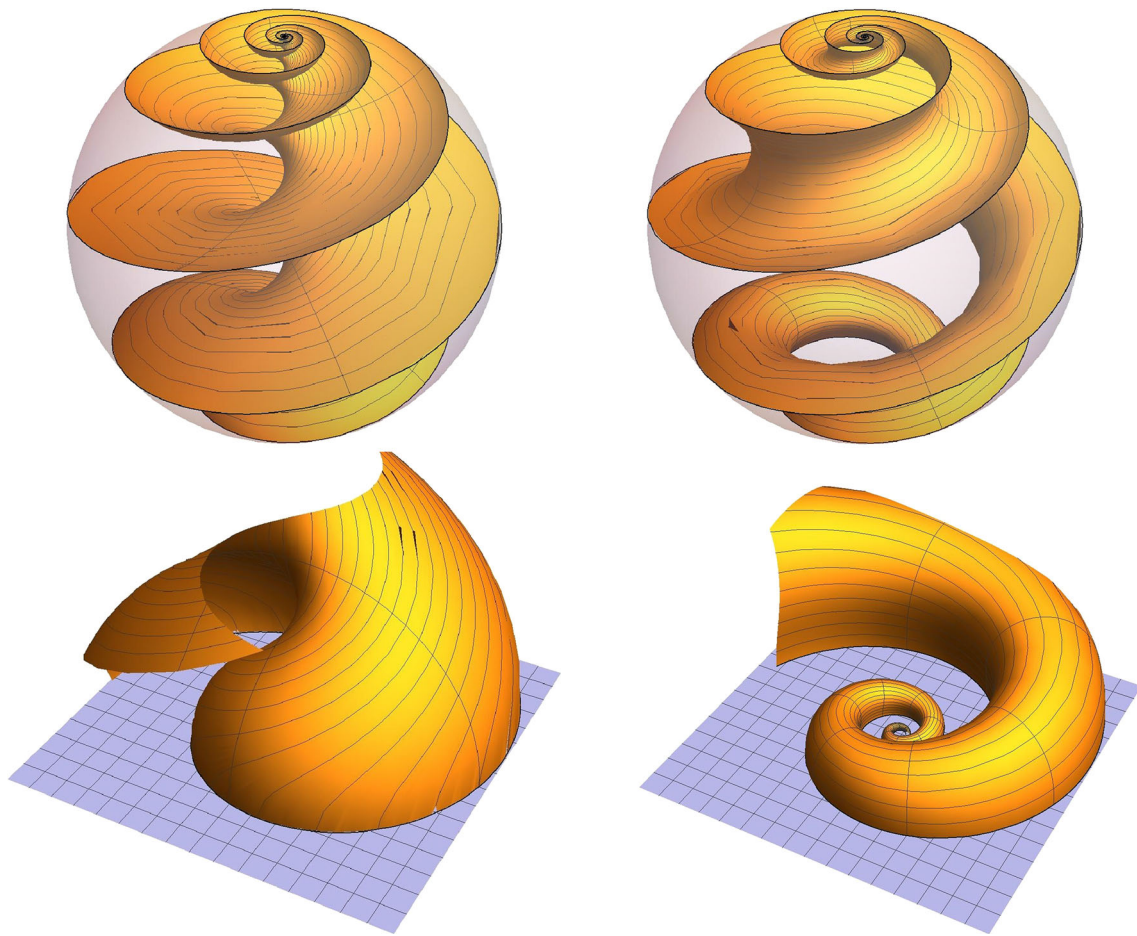
Fig. 12 Two minimal surfaces corresponding to the same boundary curve defined by $\omega = 1/4$ and $\delta\varphi = \pi$

1. When $\omega_1 > \omega_0$, $\delta\varphi$ is a monotonous function of E ranging in $[0, \pi]$. Consequently, for every angle $\delta\varphi_1$ there is a unique E, and, thus, a unique minimal surface.
2. When $\omega_1 < \omega_0$, $\delta\varphi$ is not one-to-one but it is an increasing function of E for $E < E_0$ and a decreasing function of E for $E > E_0$, and, thus, it acquires a maximum value equal to $\delta\varphi_{max} = \delta\varphi(E_0, \omega_1)$. We may distinguish two cases:

   (a) $\pi < \delta\varphi_{max} < 2\pi$. In this case, if $\delta\varphi_1 > 2\pi - \delta\varphi_{max}$, there will be three distinct values of E corresponding to an appropriate value of $\delta\varphi$ and consequently three distinct minimal surfaces. Let these values be E_1, E_2 and E_3, where $E_1 < E_2 < E_3$, then $\delta\varphi(E_1, \omega_1) = \delta\varphi_1$ and $\delta\varphi(E_{2,3}, \omega_1) = 2\pi - \delta\varphi_1$. The smaller the value of E, the more "confined" is the appearance of the surface as in the left part of Fig. 12. There is only one exception to this rule when $\delta\varphi_1 = \pi$; in this case which there are exactly two minimal surfaces, one being a helicoid. On the other hand, if $\delta\varphi_1 < 2\pi - \delta\varphi_{max}$, there will be only one solution with $E < E_0$.

   (b) $\delta\varphi_{max} > 2\pi$. In this case, there are three distinct embedding minimal surfaces for all values of $\delta\varphi_1$ with the same properties as described in the case above. Depending on the value of $\delta\varphi_1$, there may exist more minimal surfaces, coming in pairs, with self-intersections, which correspond to $\delta\varphi = 2\pi n \pm \delta\varphi_1 > 2\pi$.

Summing up, if only embedding surfaces are considered, there exist at most three selections for a minimal surface with a given entangling curve. It is quite complicated to compare analytically the parameter a_0 for elliptic surfaces with the same entangling curve to find which one is the globally preferred. As shown in Fig. 13, it turns out that the globally preferred surface is always the one with the minimum value of E, which is the only one having $\delta\varphi < \pi$. As the entangling curve separates the boundary to two unequal regions, we could say in a humorous manner that the unstable minimal surfaces have lost their way and wrapped around the wrong region of the boundary.
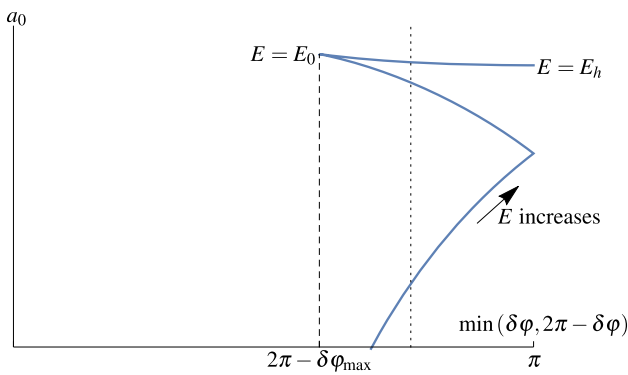
Fig. 13 The coefficient a_0 versus $\min(\delta\varphi, 2\pi - \delta\varphi)$ for $\omega = 0.25$. For this value of ω, $\pi < \delta\varphi_{\max} < 2\pi$. Points on a vertical line are surfaces with the same entangling curve

A consequence of the above is the fact that helicoids with $\omega < \omega_0$ are globally unstable. This bound coincides with the bound for the parameter ω determined in [41] for the local stability of a helicoid. From a purely mathematical point of view, in this work we made progress determining ω_0 analytically through Eq. (3.17). Moreover, we managed to find the stable minimal surface to which an unstable helicoid collapses.

As the members of an associate family of minimal surfaces share the same local stability properties and since we showed that elliptic minimal surfaces with the same value for E belong to such a family, the results of [41,42] imply that all elliptic minimal surfaces with $E < E_0$ are locally stable, whereas those with $E > E_0$ are locally unstable. This implies that comparing the three elliptic minimal surfaces with the same entangling curve, the surface with $E = E_1$ is both locally and globally stable, the surface with $E = E_2$ is locally stable but globally unstable, while the surface with $E = E_3$ is both locally and globally unstable.

5.2 Circular entangling curves

For catenoids, the boundary curve consists of two circles, which are parallel to the equator and separate the boundary sphere to three regions. As a result, there is the possibility of a geometric phase transition, between any of the two catenoid minimal surfaces corresponding to the same ratio of boundary circle radii and a Goldschmidt solution being the union of two disjoint surfaces each corresponding to a polar cap region, as those presented in [15]. Figure 14 depicts a catenoid and a Goldschmidt minimal surface sharing the same boundary conditions. This geometric phase transition
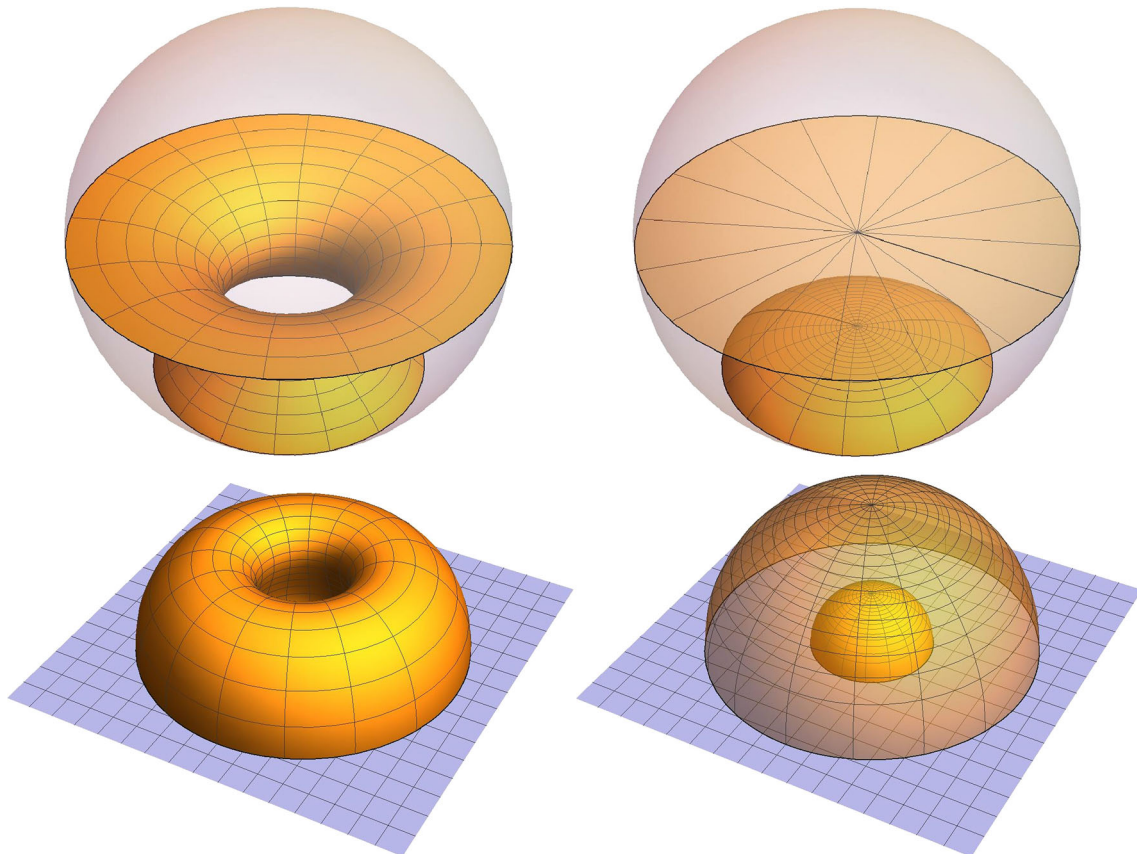

Fig. 14 A catenoid and a Goldschmidt minimal surface corresponding to the same boundary conditions
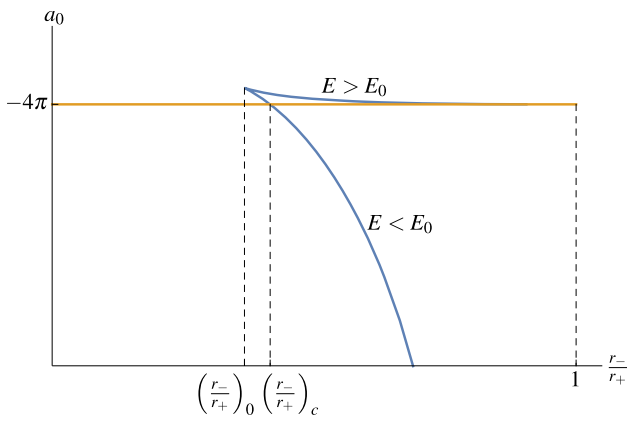
Fig. 15 The coefficient a_0^{catenoid} as a function of the ratio of the radii of the boundary circles. The singular point of the curve corresponds to $E = E_0$

has already been studied in the literature, mainly in the context of Wilson loops [43–46]. However, for completeness we study it in our language. Although the background geometry is different, the situation is similar to the usual problem of a soap bubble attached to two rings. Searching for a minimal surface in flat space that is anchored to two coaxial circles, there are three options. Two of those are portions of the catenoid and the third option is the Goldschmidt solution being the union of the two disks each being the minimal surface corresponding to a single circle boundary.

We remind that the area of the minimal surface corresponding to a polar cap region is $A = \Lambda L - 2\pi \Lambda^2$ (see for example [15]) and consequently, the area for the union of two such surfaces is given by

$$A = \Lambda L - 4\pi \Lambda^2. \tag{5.7}$$

The catenoid is preferred to the two disjoint surfaces when $a_0^{\text{catenoid}} < -4\pi$. This inequality holds when the constant E is smaller than the critical value $E_c \simeq 0.760039$ satisfying

$$\omega_1 (E_c) \frac{E_c}{6} + \zeta (\omega_1 (E_c)) = \sqrt{\frac{E_c}{2}}. \tag{5.8}$$

Consequently, since $E_c < E_0$, when the ratio of the radii of the two boundary circles is smaller than the critical value $(r_-/r_+)_c \simeq 0.416073$, the disjoint surfaces are the preferred solution, whereas, when the ratio of the radii is larger that this critical value, the catenoid corresponding to the smaller value of E for the given ratio is preferred. The catenoid corresponding to the larger value of E is never preferred in comparison to any of the other two options. Figure 15 depicts the dependence of the coefficient a_0^{catenoid} on the ratio (r_-/r_+).

6 Discussion

We constructed a family of static minimal surfaces in AdS$_4$ starting from a specific class of solutions of the Pohlmeyer reduced system, namely the Euclidean cosh-Gordon equation. This specific class comprises of solutions depending on only one of the two isothermal coordinates parametrizing the minimal surface. For these solutions, the equations of motion for the embedding functions are reduced to four pairs of effective Schrödinger problem with opposite eigenvalues, each pair consisting of a flat potential and an $n = 1$ Lamé potential. An appropriate ansatz built on one eigenfunction corresponding to the finite band and another corresponding to the finite gap of the Lamé spectrum is shown to satisfy the geometric and Virasoro constraints of the problem, and, thus, provide a family of static minimal surfaces in AdS$_4$.

The family of elliptic minimal surfaces is a two-parameter family, having as special limits the helicoids, catenoids and conical (cusp) minimal surfaces in H^3. This two-parameter family of solutions can be divided to one-parameter families each containing a single helicoid surface and either a catenoid or a conical surface and having the following properties: they are associate families of minimal surfaces and furthermore all their members correspond to a unique solution of the Pohlmeyer reduced system.

The general minimal surface corresponds to an entangling curve in the boundary being the union of two logarithmic spirals, one being the rotation of the other by a given angle. It is shown that in general there may exist more than one elliptic minimal surfaces corresponding to the same boundary conditions, allowing geometric phase transitions between them. Conditions for the global and local stability of an elliptic minimal surface are derived. Interestingly, the relevant critical values of the surface parameters are connected to the energy that a point particle moving in one dimension under the influence of a hyperbolic sine potential must have so that its "time of flight" is maximum.

The constructed surfaces, being co-dimension two minimal surfaces in AdS$_4$, have particular interest in the framework of holographic duality, since their area is connected to the entanglement entropy in the boundary CFT through the Ryu–Takayanagi conjecture. Unlike the minimal surfaces typically used in the literature, namely those corresponding to a disk or an infinite strip region in the boundary, these surfaces are anchored to entangling curves characterized by non-trivial curvature. As such, they can provide a useful tool in the study of the relation between entanglement entropy and the geometric characteristics of the entangling curve [39,47]. Furthermore, the discovered geometric phase transitions between different minimal surfaces can provide light in the role of entanglement entropy as an order parameter in confinement/deconfinement phase transitions.

An important result in the program of holographic entanglement entropy is the equivalence of the first law of entanglement thermodynamics to Einstein equations at linear order [13,14]. Nevertheless, these results are based on calculations using "semi-spherical" minimal surfaces corresponding to

spherical entangling curves, which are special in two ways: First, the entangling curve has constant curvature. Second, the minimal surface does not just have vanishing mean curvature, but both principal curvatures vanish; they are the analog of a plane in hyperbolic space. Since the holographic calculation of the variations of entanglement entropy strongly depends on the geometric characteristics of the minimal surface, verification of this results making use of elliptic minimal surfaces will greatly support the idea of gravity being an emergent entropic force related to quantum entanglement statistics. Furthermore, such calculations are interesting in terms of the stress-energy/Cotton tensor duality appearing in AdS_4 metric perturbations and the appropriate prescription that has to be attached to Ryu–Tanayanagi conjecture, so that it is valid in the case of perturbations obeying non-Dirichlet boundary conditions [15].

The presented techniques are generalizable to higher dimensions, where Pohlmeyer reduction results in multi-component integrable systems of the sinh-Gordon family. Unfortunately, such minimal surfaces will not be co-dimension two surfaces and consequently will not be interesting in the context of Ryu–Takayanagi conjecture, but only from a more mathematical point of view. On the contrary, generalizations of the constructed elliptic minimal surfaces in AdS_4 involving more general linear combinations of the Lamé eigenfunctions can lead to the construction of minimal surfaces with interesting geometric characteristics and potential applications in holographic entanglement entropy.

Appendix A: Useful formulas for the Weierstrass functions

The Weierstrass function $\wp$ is an elliptic (doubly periodic) function of one complex variable which satisfies the equation

$$\left(\frac{d\wp}{dz}\right)^2 = 4\wp^3 - g_2\wp - g_3. \tag{A.1}$$

The periods of $\wp$ are connected with the roots of the cubic polynomial

$$Q(y) = 4y^3 - g_2 y - g_3. \tag{A.2}$$

Let the three roots be e_1, e_2 and e_3. The absence of a quadratic term implies that the roots satisfy $e_1 + e_2 + e_3 = 0$. In the following we concentrate on the case that all three roots are real. We order the roots so that $e_1 > e_2 > e_3$. Then the fundamental periods of the function $\wp$ are a real one $2\omega_1$ and an imaginary one $2\omega_2$ which are related to the roots as follows:

$$\omega_1 = \frac{K(k)}{\sqrt{e_1 - e_3}}, \quad \omega_2 = \frac{i\,K(k')}{\sqrt{e_1 - e_3}}, \tag{A.3}$$

where $K(k)$ is the complete elliptic integral of the first kind and

$$k^2 = \frac{e_2 - e_3}{e_1 - e_3}, \quad k'^2 = \frac{e_1 - e_2}{e_1 - e_3}, \quad k^2 + k'^2 = 1. \tag{A.4}$$

The Weierstrass function $\wp$ obeys the half-period relations,

$$\wp(\omega_1) = e_1, \quad \wp(\omega_2) = e_3, \quad \wp(\omega_3) = e_2, \tag{A.5}$$

where $\omega_3 := \omega_1 + \omega_2$.

As long as all three roots are real, Eq. (A.1) has two real solutions in the real domain,

$$y_1(x) = \wp(x), \tag{A.6}$$

$$y_2(x) = \wp(x + \omega_2), \tag{A.7}$$

the first one being unbounded and ranging between e_1 and $+\infty$ and the second one being bounded and ranging between e_3 and e_2. In the opposite case, there is only one unbounded real solution in the real domain.

The Weierstrass ζ function is a doubly quasi-periodic function, which is defined so that

$$\frac{d\zeta}{dz} = -\wp. \tag{A.8}$$

Finally, the Weierstrass σ function obeys the defining relation

$$\frac{1}{\sigma}\frac{d\sigma}{dz} = \zeta. \tag{A.9}$$

The Weierstrass elliptic function $\wp$ is an even function of z, while Weierstrass functions ζ and σ are odd functions of z,

$$\wp(-z) = \wp(z), \tag{A.10}$$

$$\zeta(-z) = -\zeta(z), \tag{A.11}$$

$$\sigma(-z) = -\sigma(z). \tag{A.12}$$

As mentioned above, the functions ζ and σ are not periodic. Under a shift of the complex variable z in the lattice

defined by the periods of $\wp$, they transform as

$$\wp\left(z + 2m\omega_1 + 2n\omega_2\right) = \wp\left(z\right), \tag{A.13}$$

$$\zeta\left(z + 2m\omega_1 + 2n\omega_2\right) = \zeta\left(z\right) + 2m\zeta\left(\omega_1\right) + 2n\zeta\left(\omega_2\right), \tag{A.14}$$

$$\sigma\left(z + 2m\omega_1 + 2n\omega_2\right)$$
$$= (-1)^{m+n+mn} e^{\left(2m\zeta(\omega_1)+2n\zeta(\omega_2)\right)\left(z+m\omega_1+n\omega_2\right)}\sigma\left(z\right). \tag{A.15}$$

The quantities $\zeta\left(\omega_1\right)$ and $\zeta\left(\omega_2\right)$ obey the non-trivial relation

$$\omega_2\zeta\left(\omega_1\right) - \omega_1\zeta\left(\omega_2\right) = i\frac{\pi}{2}. \tag{A.16}$$

The Weierstrass functions obey the homogeneity relations,

$$\wp\left(z; g_2, g_3\right) = \mu^2\wp\left(\mu z; \frac{g_2}{\mu^4}, \frac{g_3}{\mu^6}\right), \tag{A.17}$$

$$\zeta\left(z; g_2, g_3\right) = \mu\zeta\left(\mu z; \frac{g_2}{\mu^4}, \frac{g_3}{\mu^6}\right), \tag{A.18}$$

$$\sigma\left(z; g_2, g_3\right) = \frac{1}{\mu}\sigma\left(\mu z; \frac{g_2}{\mu^4}, \frac{g_3}{\mu^6}\right). \tag{A.19}$$

Choosing $\mu = i$, the homogeneity relations yield

$$\wp\left(z; g_2, g_3\right) = -\wp\left(iz; g_2, -g_3\right), \tag{A.20}$$

$$\zeta\left(z; g_2, g_3\right) = i\zeta\left(iz; g_2, -g_3\right), \tag{A.21}$$

$$\sigma\left(z; g_2, g_3\right) = -i\sigma\left(iz; g_2, -g_3\right), \tag{A.22}$$

which imply that on the imaginary axis of the z plane, $\wp$ is real, whereas ζ and σ are imaginary.

As an elliptic function, $\wp$ possesses an addition formula. The functions ζ and σ are not elliptic, however, they also possess similar properties,

$$\wp\left(z + w\right) = -\wp\left(z\right) - \wp\left(w\right) + \frac{1}{4}\left(\frac{\wp'\left(z\right) - \wp'\left(w\right)}{\wp\left(z\right) - \wp\left(w\right)}\right)^2, \tag{A.23}$$

$$\zeta\left(z + w\right) = \zeta\left(z\right) + \zeta\left(w\right) + \frac{1}{2}\frac{\wp'\left(z\right) - \wp'\left(w\right)}{\wp\left(z\right) - \wp\left(w\right)}, \tag{A.24}$$

$$\wp\left(z\right) - \wp\left(w\right) = -\frac{\sigma\left(z - w\right)\sigma\left(z + w\right)}{\sigma^2\left(z\right)\sigma^2\left(w\right)}. \tag{A.25}$$

Applying the last formula in the special case w coincides with any of the half-periods yields

$$\wp\left(z\right) - e_{1,3,2} = -\frac{\sigma\left(z + \omega_{1,2,3}\right)\sigma\left(z - \omega_{1,2,3}\right)}{\sigma^2\left(z\right)\sigma^2\left(\omega_{1,2,3}\right)}. \tag{A.26}$$

Finally, the Weierstrass functions obey the following integral formula:

$$\wp'\left(a\right)\int\frac{\mathrm{d}z}{\wp\left(z\right) - \wp\left(a\right)} = 2\zeta\left(a\right)z + \ln\frac{\sigma\left(z - a\right)}{\sigma\left(z + a\right)}. \tag{A.27}$$

References

1. J.M. Maldacena, The large N limit of superconformal field theories and supergravity. Adv. Theor. Math. Phys. **2**, 231 (1998). arXiv:hep-th/9711200
2. S.S. Gubser, I.R. Klebanov, A.M. Polyakov, Gauge theory correlators from noncritical string theory. Phys. Lett. B **428**, 105 (1998). arXiv:hep-th/9802109
3. E. Witten, Anti-de Sitter space and holography. Adv. Theor. Math. Phys. **2**, 253 (1998). arXiv:hep-th/9802150
4. E.P. Verlinde, On the origin of gravity and the laws of Newton. JHEP **1104**, 029 (2011). arXiv:1001.0785 [hep-th]
5. S. Ryu, T. Takayanagi, Holographic derivation of entanglement entropy from AdS/CFT. Phys. Rev. Lett. **96**, 181602 (2006). arXiv:hep-th/0603001
6. S. Ryu, T. Takayanagi, Aspects of holographic entanglement entropy. JHEP **0608**, 045 (2006). arXiv:hep-th/0605073
7. V.E. Hubeny, M. Rangamani, T. Takayanagi, A covariant holographic entanglement entropy proposal. JHEP **0707**, 062 (2007). arXiv:0705.0016 [hep-th]
8. T. Nishioka, S. Ryu, T. Takayanagi, Holographic entanglement entropy: an overview. J. Phys. A **42**, 504008 (2009). arXiv:0905.0932 [hep-th]
9. M. Van Raamsdonk, Comments on quantum gravity and entanglement. arXiv:0907.2939 [hep-th]
10. M. Van Raamsdonk, Building up spacetime with quantum entanglement. Gen. Relativ. Gravit. **42**, 2323 (2010). arXiv:1005.3035 [hep-th]
11. T. Takayanagi, Entanglement entropy from a holographic viewpoint. Class. Quantum Gravity **29**, 153001 (2012). arXiv:1204.2450 [gr-qc]
12. H. Casini, M. Huerta, R.C. Myers, Towards a derivation of holographic entanglement entropy. JHEP **1105**, 036 (2011). arXiv:1102.0440 [hep-th]
13. N. Lashkari, M.B. McDermott, M. Van Raamsdonk, Gravitational dynamics from entanglement thermodynamics. JHEP **1404**, 195 (2014). arXiv:1308.3716 [hep-th]
14. T. Faulkner, M. Guica, T. Hartman, R.C. Myers, M. Van Raamsdonk, Gravitation from entanglement in holographic CFTs. JHEP **1403**, 051 (2014). arXiv:1312.7856 [hep-th]
15. I. Bakas, G. Pastras, Entanglement entropy and duality in AdS$_4$. Nucl. Phys. B **896**, 440 (2015). arXiv:1503.00627 [hep-th]
16. K. Pohlmeyer, Integrable Hamiltonian systems and interactions through quadratic constraints. Commun. Math. Phys. **46**, 207 (1976)
17. V.E. Zakharov, A.V. Mikhailov, Relativistically invariant two-dimensional models in field theory integrable by the inverse problem technique. (In Russian). Sov. Phys. JETP **47**, 1017 (1978) [Zh. Eksp. Teor. Fiz. **74**, 1953 (1978)]
18. H. Eichenherr, K. Pohlmeyer, Lax pairs for certain generalizations of the sine-Gordon equation. Phys. Lett. B **89**, 76 (1979)
19. K. Pohlmeyer, K.H. Rehren, Reduction of the two-dimensional O(n) nonlinear σ-model. J. Math. Phys. **20**, 2628 (1979)
20. H. Eichenherr, J. Honerkamp, Reduction of the CP^N nonlinear σ model. J. Math. Phys. **22**, 374 (1981)
21. I. Bakas, Conservation laws and geometry of perturbed coset models. Int. J. Mod. Phys. A **9**, 3443 (1994). arXiv:hep-th/9310122
22. I. Bakas, Q.H. Park, H.J. Shin, Lagrangian formulation of symmetric space sine-Gordon models. Phys. Lett. B **372**, 45 (1996). arXiv:hep-th/9512030
23. C.R. Fernandez-Pousa, M.V. Gallas, T.J. Hollowood, J.L. Miramontes, The symmetric space and homogeneous sine-Gordon theories. Nucl. Phys. B **484**, 609 (1997). arXiv:hep-th/9606032
24. J.L. Miramontes, Pohlmeyer reduction revisited. JHEP **0810**, 087 (2008). arXiv:0808.3365 [hep-th]

25. B.M. Barbashov, V.V. Nesterenko, Relativistic string model in a space-time of a constant curvature. Commun. Math. Phys. **78**, 499 (1981)

26. H.J. De Vega, N.G. Sanchez, Exact integrability of strings in D-dimensional De Sitter space-time. Phys. Rev. D **47**, 3394 (1993)

27. A.L. Larsen, N.G. Sanchez, Sinh-Gordon, cosh-Gordon and Liouville equations for strings and multistrings in constant curvature space-times. Phys. Rev. D **54**, 2801 (1996). arXiv:hep-th/9603049

28. M. Grigoriev, A.A. Tseytlin, Pohlmeyer reduction of $AdS_5 \times S^5$ superstring sigma model. Nucl. Phys. B **800**, 450 (2008). arXiv:0711.0155 [hep-th]

29. A. Mikhailov, S. Schafer-Nameki, Sine-Gordon-like action for the superstring in $AdS_5 \times S^5$. JHEP **0805**, 075 (2008). arXiv:0711.0195 [hep-th]

30. M. Grigoriev, A.A. Tseytlin, On reduced models for superstrings on $AdS_n \times S^n$. Int. J. Mod. Phys. A **23**, 2107 (2008). arXiv:0806.2623 [hep-th]

31. R.C. Rashkov, A note on the reduction of the $AdS_4 \times CP^3$ string sigma model. Phys. Rev. D **78**, 106012 (2008). arXiv:0808.3057 [hep-th]

32. I. Bakas, G. Pastras, On elliptic string solutions in AdS_3 and dS_3. JHEP **1607**, 070 (2016). arXiv:1605.03920 [hep-th]

33. M. Kruczenski, Spiky strings and single trace operators in Gauge theories. JHEP **0508**, 014 (2005). arXiv:hep-th/0410226

34. M. Babish, A. Bobenko, Willmore tori with umbilic lines and minimal surfaces in hyperbolic space. Duke Math. J. **72**(1), 151

35. R. Ishizeki, M. Kruczenski, S. Ziama, Notes on Euclidean Wilson loops and Riemann theta functions. Phys. Rev. D **85**, 106004 (2012). arXiv:1104.3567 [hep-th]

36. M. Kruczenski, S. Ziama, Wilson loops and Riemann theta functions II. JHEP **1405**, 037 (2014). arXiv:1311.4950 [hep-th]

37. L. Bombelli, R.K. Koul, J. Lee, R.D. Sorkin, A quantum source of entropy for black holes. Phys. Rev. D **34**, 373 (1986)

38. M. Srednicki, Entropy and area. Phys. Rev. Lett. **71**, 666 (1993). arXiv:hep-th/9303048

39. P. Bueno, R.C. Myers, Corner contributions to holographic entanglement entropy. JHEP **1508**, 068 (2015). arXiv:1505.07842 [hep-th]

40. S.S. Gubser, I.R. Klebanov, A.M. Polyakov, A Semiclassical limit of the Gauge/string correspondence. Nucl. Phys. B **636**, 99 (2002). arXiv:hep-th/0204051

41. B. Wang, Stability of helicoids in hyperbolic three-dimensional space. arXiv:1502.04764 [math.DG]

42. B. Wang, Least area spherical catenoids in hyperbolic three-dimensional space. arXiv:1204.4943 [math.DG]

43. D.J. Gross, H. Ooguri, Aspects of large N Gauge theory dynamics as seen by string theory. Phys. Rev. D **58**, 106002 (1998). arXiv:hep-th/9805129

44. K. Zarembo, Wilson loop correlator in the AdS/CFT correspondence. Phys. Lett. B **459**, 527 (1999). arXiv:hep-th/9904149

45. N. Drukker, B. Fiol, On the integrability of Wilson loops in $AdS_5 \times S^5$: some periodic ansatze. JHEP **0601**, 056 (2006). arXiv:hep-th/0506058

46. A. Dekel, T. Klose, Correlation function of circular Wilson loops at strong coupling. JHEP **1311**, 117 (2013). arXiv:1309.3203 [hep-th]

47. S.N. Solodukhin, Entanglement entropy, conformal invariance and extrinsic geometry. Phys. Lett. B **665**, 305 (2008). arXiv:0802.3117 [hep-th]